View metadata, citation and similar papers at core.ac.uk

brought to you by CORE

provided by The University of Utah: J. Willard Marriott Digital Library

STATE-BASED PERIDYNAMICS SIMULATION OF HYDRAULIC FRACTURE PHENOMENON IN GEOLOGICAL MEDIA

by

Siavash Nadimi

A thesis submitted to the faculty of
The University of Utah
in partial fulfillment of the requirements for the degree of

Master of Science

Department of Mining Engineering

The University of Utah

December 2015

Copyright © Siavash Nadimi 2015

All Rights Reserved

The University of Utah Graduate School

STATEMENT OF THESIS APPROVAL

The following faculty members served as the supervisory committee chair and members for the thesis of Siavash Nadimi.

Dates at right indicate the members' approval of the thesis.

Ilija Miskovic, Chair	July 29, 2015 Date Approved
Michael G. Nelson, Member	July 29, 2015 Date Approved
John D. McLennan, Member	July 29, 2015 Date Approved

The thesis has also been approved by Michael G. Nelson Chair of the Department/School/College of Mining Engineering and by David B. Kieda, Dean of The Graduate School.

ABSTRACT

Tight shale reservoirs have recently emerged as potential game changers in oil and gas and energy sectors worldwide. Consequently, exploration and exploitation of unconventional reservoirs has significantly increased over the last decade. Currently used stimulation designs are based on conventional planar fracture models that cannot realistically simulate the geometry and the extent of hydraulically induced fractures. For that reason, developing models that can thoroughly and accurately describe fracture network initiation and propagation plays a significant role in evaluating well production.

The main goal of this work is to evaluate the utility of the peridynamic theory (PD) in modeling the process of hydraulic fracturing. Peridynamics is a nonlocal theory of continuum media that can facilitate a direct coupling between classical continuum mechanics and molecular dynamics. A linear-viscoelastic PD model was applied to a three-dimensional domain that was discretized with cubic lattices of particles. Damage in the model is represented by the bond breakage; as the stretch between two lattices reaches its critical limit, s_0, the bond breaks.

The validity of the peridynamic simulation was tested by comparing results obtained in this project against the results obtained in a study performed by Zhou et al. Therefore, six sets of experimental tests were conducted to simulate hydraulic fracturing based on the peridynamic method. Five sets of the simulation results produced in this work were in good agreement with the experimental results. The investigation examined the

influences of the differential horizontal stress and preexisting fracture, along with different approach angles, on the geometry of the hydraulic fracture.

Different injection rates were applied to the model in order to compare the fractured area that resulted from different injection rates. The simulation showed that the maximum dilatation and fractured zone occurred at the injection rate of 0.61 m^3⁄min. The 0.61 m^3/min injection rate caused the highest complete damage (0.9–1) with 5.24 % of the total number of atoms. As a result, the peridynamic approach presents promising results in predicting fracture propagation and damage area.

To My love, Mahsa

To my family

For their love, support, and encouragement

TABLE OF CONTENTS

LIST OF FIGURES

Figure Page

LIST OF TABLES

Table Page

ACKNOWLEDGEMENTS

I owe a debt of gratitude and would like to express my sincere appreciation to my advisor, Dr. Ilija Miskovic, for his precious guidance and suggestions. I pay homage to my professor for the opportunities, facilities, and financial support that I was offered in his research group during my master's program. I thank my committee members Dr. Michael G. Nelson and Dr. John D. McLennan for providing valuable suggestions. In addition, thank you to the CHPC teams for providing high-performance computing tools.

I would like to acknowledge my dear colleagues and friends Mr. Jan Goral, Mr. Gorakh Pawar, Mr. Behzad Vaziri Hassas, Mr. Alireza Samimi, Mr. Ahmad Rezazadeh, and Mr. Hossein Dadkhah for their kind cordiality and affability during my years of living abroad. Appreciation is also extended to the Department of Mining Engineering for providing the opportunity of using equipment and laboratories. I also thank Pam Hofmann and Samantha Davis for their support during my graduate career.

Finally, I also would like to express my most warmest and sincere appreciation to my love Mahsa, my mother Shademan, my father Behrouz, and also to my siblings, Mehrnoush, Kianoush, and Sanaz for their virtuous spiritual and pecuniary supports and encouragement.

CHAPTER 1

INTRODUCTION AND OBJECTIVE

1.1 Introduction

The problems related to discontinuities are very important in the field of rock mechanics. Several models have been developed in the past to investigate the characteristics of discontinuities; however, predicting the fracture path and its characteristics remains an open problem, confirmed by many experimental studies (Gu et al., 2011; McLennan et al., 2010; Nadimi et al., 2011). Different classes of models are used widely to simulate the fracturing process in solid materials, including continuum-based models, discrete element models, and molecular dynamic (MD) models.

One of the most notable challenges in the simulation of geomechanical problems by molecular dynamic theory is the size of the simulation. Crack propagation is dramatically influenced by stress conditions since the MD model should simulate all of these stress waves. Accordingly, atomistic or molecular simulation is a time-consuming and computationally expensive method, making it unsuitable for investigating macroscopic crack propagation.

The discrete element method (DEM) was developed for simulating discontinuous media. Characteristics of discontinuities such as the locations, orientations, and dimensions of the fractures (except for some major fractures) are among the most significant problems

associated with DEM. In addition, in a DEM model, the sub-block deformation in the simulation domain creates no strain inside the sub-block; rather, it produces a displacement of sub-blocks, often on a large scale (Jing & Stephansson, 2007).

Continuum models do not have the ability to predict crack propagation as it actually occurs. To overcome these limitations, some concepts, such as the cohesive-zone, were added to the classical continuum method to make it capable of capturing the failure process (Barenblatt, 1962). In the continuum-based approach, the cohesive zone concept modifies the classical continuum mechanics equations and introduces an internal length scale. In the extended finite element method (XFEM) for modeling the fracturing process, a damage criterion and tracking formulation of the stresses around the crack-tip are needed. Material failure is defined based on a scalar parameter called "damage" in which bonds between material points break. A preexisting crack in the realm of linear elastic fracture mechanics (LEFM) is necessary in order to model the cracking in a solid material. Stresses at the crack-tip are mathematically singular. Therefore, an external criterion such as the critical energy release rate, which is not a part of the governing equations of classical continuum mechanics, is necessary to treat the crack initiation and growth. Furthermore, crack nucleation within the LEFM method still remains an open problem (Belytschko et al., 2003; Bishop et al., 2012; Camacho & Ortiz, 1996; Chen & Gunzburger, 2011; Ha & Bobaru, 2011; Nadimi et al., 2013; Ortiz & Pandolfi, 1999; Rabczuk & Belytschko, 2004; Song et al., 2006; F. Zhou & Molinari, 2004).

In addition, locality is the principal assumption in continuum theory. In classical continuum theory, a material particle only interacts with its immediate neighbors. Therefore, in continuum models, a material particle exchanges mass, momentum, and energy only with its immediate neighbors. In general, at the macro-scale, this assumption

might be acceptable, but it is questionable and cannot be applied when microscopic features are considered (Madenci & Oterkus, 2014; Warren et al., 2009)

Peridynamic theory was developed by Silling (1998), and was initially used for investigating deformation in discontinuous media, especially fractures. Peridynamics is a nonlocal theory that bridges classical continuum mechanics and molecular dynamics (Madenci & Oterkus, 2014; Silling, 1998). However, the main difference between classical continuum theory and the peridynamic theory is that in the former, the partial differential equations are replaced by integral equations. Since the displacement derivatives are not included in peridynamics method, it is possible to compute the displacements everywhere, whether or not discontinuities are present (Askari et al., 2008; Ha & Bobaru, 2011; Kilic, 2008; Madenci & Oterkus, 2014; Taylor & Steigmann, 2013).

The peridynamic approach provides a mathematical method that includes the concepts of nonlinearity in kinematic and material response, fracture, damage, and surface effects. Damage is incorporated into the model through the bond breakage when the strains exceed the critical value. Once a bond breaks, it cannot sustain forces any longer (Turner, 2013; Warren et al., 2009).

The peridynamic theory has been successfully used to model and simulate damage (Demmie & Silling, 2007; Gerstle et al., 2010; Kilic & Madenci, 2009; Taylor & Steigmann, 2013). Peridynamics was used to simulate the Kallthoff-Winkler experiment in which an impactor hits a plate including two parallel notches (Silling, 2003). The simulation successfully predicted the crack growth angle in the plate. Later, Silling and Askari (2005) used the peridynamic theory to predict the impact damage in a plate with a central crack. Recently, the peridynamic theory was applied to model the interaction between the fluid and the surface of the fracture in the context of hydraulic fracturing

(Silling & Askari, 2005; Turner, 2013). The peridynamic theory was also used by Askari et al. to simulate multiscale materials (Askari et al., 2008). The pairwise moments were added into peridynamics model in order to model the quasi-static behavior of the concrete structures (Gerstle et al., 2007a; Gerstle et al., 2009).

In this thesis, the peridynamic theory was used to investigate hydraulic fracturing initiation and propagation in a geological formation, using. The state-based viscoelastic peridynamic approach to simulate the phenomenon. The interaction between induced fractures and a preexisting fracture, as well as the influence of the angle of approach and differential horizontal stress on the fracture propagation behavior, was investigated through the simulation. Finally, the applicability of the model to predict the hydraulic fracture process was evaluated, and the fractured area of three different injection rates was compared.

1.2 Objective

The purpose of this thesis is to simulate the hydraulic fracturing phenomena using the peridynamic theory. First, the utility of the peridynamic theory for simulating the fracturing process based on hydraulic loading was evaluated. Then, PDLAMMPS open source software was used to simulate hydraulic fracturing initiation and propagation based on the state-based peridynamic method. In order to reach this primary objective, the following tasks were identified and performed:

- Review the applications of the peridynamic theory for modeling various problems;
- Evaluate the application of the peridynamic theory for simulating the hydraulic

fracture process;

- Implement the viscoelastic behavior parameters;
- Verify and calibrate the model by using the experimental tests results conducted by Zhou et al. (2008);
- Simulate the hydraulic fracture process in a heterogonous medium;
- Simulate the fracture initiation and propagation through a hydraulic fracture block by applying different injection rates.

1.3 Methodology

In this thesis, the peridynamic theory was chosen to simulate the fracturing process under hydraulic loading. Therefore, the state-based peridynamic theory was used to simulate the phenomenon. PDLAMMPS open source software was used to simulate the hydraulic fracturing phenomena in a geological formation. This software was developed using the peridynamic model, discretized within LAMMPS. A detailed description of the approach is given below:

- Modeled a cube geometry in the 3D domain, under vertical and horizontal compressive stresses, based on the peridynamic theory, using PDLAMMPS open source software for coding the simulation.
- The peridynamic viscoelasticity formulation was used in this work to simulate behavior of the geological formation. The material behavior was presented to the model based on the viscoelastic behavior of the geological formation. Then, boundary conditions were applied to the simulation domain.
- The material behavior and peridynamics-related parameters were verified, and

the accurate simulation parameters, based on the material behavior and previous studies, were determined.

- A perforation hole in the model was created and water pressure applied to the hole. The pressure initiated damage and fractures around the hole through the simulation.
- Model damage was computed based on the damage per atom and dilatation per atom.

1.4 Scope

This thesis includes six chapters. Following Chapter 1, Introduction and Objectives is Chapter 2, which discusses unconventional reservoirs, hydraulic fracturing processes, and the common numerical methods that have been historically used for simulating hydraulic fracturing phenomenon. Chapter 3 provides a literature review of peridynamic theory and its applications in different fields. Chapter 4 describes the design of hydraulic fracturing simulation in the PDLAMMPS software based on the peridynamic theory and the validation approach used to evaluate the model. Chapter 5 presents the results of the simulation and provides a discussion thereof. Finally, Chapter 6 provides conclusions and suggests related future research that could be conducted.

CHAPTER 2

LITERATURE REVIEW

This chapter contains three main sections. Section 2.1 presents a literature review of hydraulic fracture and unconventional reservoirs with basic concepts of the hydraulic fracture initiation and propagation summarized in Section 2.2. Sections 2.3 and 2.4 describe the basic concepts and common methods used for modeling and simulating the hydraulic fracture phenomenon.

2.1 Unconventional Reservoirs

The term "unconventional reservoir" is used to describe many types of hydrocarbon-bearing formations and reservoirs from which economic production of hydrocarbons is not possible without stimulation. Commonly, "unconventional" reservoirs include: tight-gas sandstones, gas hydrates, oil shale formations, heavy oil sandstones, and shale gas formations. Shale is composed of fine-grained particles less than four microns in diameter. Shales are commonly comprised of clay, quartz, feldspar, and heavy minerals (Passey et al., 2010a). The vertical heterogeneity in shale reservoirs can be related to the geological and biotic conditions in which sediments were deposited. The systematic variation of the source rock properties in vertical and lateral directions arises because of the depositional environment and stratal sedimentation. In addition, variation is tied back

to accumulation of the entire stratal units. Moreover, systematic changes also occur in lateral direction. Most existing shale gas reservoirs originate in organic-rich mud (Morris, 1980). Mineral composition in shale reservoirs significantly affects geomechanical properties of shale. As shown in Figure 2.1, the mineral composition is different in each shale gas reservoir (Passey et al., 2010a).

From a simulation point of view, not all forms of quartz have the same effects in shale gas reservoirs. The crystallization that forms different framework of quartz cement affects the permeability of a formation. Mineralogical variation in shale occurs down in the millimeters and centimeters scale (Passey et al., 2010b).

2.2 Hydraulic Fracturing

The low matrix permeability of tight-gas shale formations (in the nano- to microdarcy range) implies that successful economical production depends on the existence of effective conductivity. Because of the low matrix permeability, one needs to enhance the tight formation's productivity by inducing a fracture network in order to allow gas to be transported to the wellbore for production. To increase the number of intersections between induced and preexisting fractures, large hydraulic fracture stimulations are typically required (Bai, Green, & Suarez-Rivera, 2005; Suarez-Rivera, Handwerger, Kieschnick, Martin, & Green, 2005). "*Hydraulic fracturing can be broadly defined as the process by which a fracture initiates and propagates due to hydraulic loading (i.e., pressure) applied by a fluid inside the fracture*" (Valk & Economides, 1995). Simply described, hydraulic fracturing involves three processes: (i) mechanical deformation due to fluid pressure; (ii) fluid flow within the fracture; and (iii) fracture propagation (Adachi, Siebrits, Peirce, & Desroches, 2007; Zoback, Rummel, Jung, & Raleigh, 1977).

There are different hydraulic fracture models used to predict fracture propagation geometry. They are mainly classified as 2D and 3D models. The Perkins-Kern-Nordgren (PKN) fracture model, the Khristianovic-Geertsma-de Klerk (KGD) fracture model, and the Penny-shape (radial model) (see Figure 2.2) (Valk & Economides, 1995) are all 2D models used for simulating the hydraulic fracturing process.

The group of 3D models includes both fully-3D models and pseudo-three-dimensional (P-3D) models (see Figure 2.3). In the P-3D model, height is calculated as a function of the lateral position of the fracture in every time step controlled by the pressure (Valkó & Economides, 1995; Xiang, 2011; Yew, 1997).

Perkins and Kern developed a formula to compute the fracture propagation length and width with a fixed height. Later, Nordgren developed a model by adding fluid loss to the solution. Hence, the model is commonly called PKN (Valk & Economides, 1995). For the PKN model, fracture toughness is negligible because the required energy for fracture propagation is significantly less than that required for fluid to flow along the fracture length and because of the plane strain behavior in the vertical direction. In addition, the fracture has a constant height and propagates along the horizontal direction. The PKN model considers plane strain in the vertical direction, and it was assumed that rock behavior in each vertical section is independent from its neighboring vertical planes. The fluid flow problem is considered in one dimension, in an elliptical channel in which the fluid pressure is supposed to be constant in each vertical cross section perpendicular to the direction of propagation (Valkó & Economides, 1995; Yew, 1997).

For the KGD model, fracture mechanics affects the fracture tip, and the flow rate and pressure in the fracture is assumed constant along the majority of the fracture length. In addition, the fracture is in a horizontal plane strain condition. It is further assumed that

the fracture tip is a cusp-shaped tip. The Penny-shaped model assumed a symmetrical fracture geometry with respect to the axe of the wellbore (Valkó & Economides, 1995; Xiang, 2011; Yew, 1997).

The 2D fracture models are limited, as they require some parameters be specified for the geometry of the fracture. Therefore, pseudo-3D approaches were developed to solve these problems by introducing variable fracture height to the models. In pseudo-3D models, height is a function of the position along the fracture and simulation time (Valkó & Economides, 1995; Yew, 1997). Due to the simplicity of the P-3D model in determining fracture height, it is widely used in the oil industry.

Numerical simulation of the hydraulic fracturing phenomenon that models the actual process is very difficult. According to previous studies, in the hydraulic fracturing process with high rock toughness fluid flows very close behind the crack tip; thus, the crack tip and the fluid front propagate together. On the other hand, in conditions of low toughness, there is a gap between the crack tip and the fluid front, so the fluid only travels through a portion of the crack length (Garagash, 2006; Hunsweck, Shen, & Lew, 2013; Lecampion & Detournay, 2007). Interaction between the fracturing fluid and the fracturing surface, the mechanical state of the rock, and coupling of the porous media with the fluid, are additional parameters that have significant effects on hydraulic fracturing modeling. Therefore, a detailed understanding of the process and modeling the actual conditions would improve the interpretation and results of the simulation.

Continuum models have been commonly used for solving coupled hydro-mechanical problems; however, identifying discontinuities in these models is very difficult. DEM is an alternative approach for addressing the coupled hydraulic fracturing process, including pore structure and fracture propagation. However, even DEM has some

drawbacks that cause difficulties in simulating the hydraulic fracture process, such as: time-consuming and expensive simulations, as well as the characterizing of discontinuities and remeshing around the crack propagation (Hunsweck et al., 2013).

2.2.1 Fracture Initiation

Fracture initiation from a borehole can be described in two ways. In the first approach, known as tensile breakdown criteria, fractures initiate at the wall of the wellbore as the hydraulic load exceeds a certain stress level (Valk & Economides, 1995). The second approach assumes that small defects are present in the rock in the form of microfractures, which lead to fracture initiation at the tip of a microfracture when the stress intensity factor exceeds a threshold value, known as fracture toughness. In fact, the latter approach is a propagation criterion applied to an initial microfracture case (Weijers, 1995). In the following subchapters, the mechanism of hydraulic fracturing is explained.

2.2.1.1 Tensile breakdown. An infinitely long borehole was considered along the Z direction with radius r_w, and fluid pressure p_w (Weijers, 1995). Two perpendicular external stresses (principle stresses) σ_{22} and σ_{33} are applied to the borehole, and the σ_{11} is parallel to the borehole direction. The applied p_w fluid pressure causes tangential stress component $\sigma_{\theta\theta}$ to decrease. Based on Kirsch's solution, the fracture initiation criterion is defined by Hubbert and Willis. Assuming linear elastic rock behavior, a fracture initiates on the surface of the borehole when the effective tangential stress exceeds the tensile strength σ_t of the host rock:

$$\sigma_{\theta\theta,e}(r_w) = -\sigma_t \qquad \text{(EQ 2. 1)}$$

Schmitt and Zoback (1989) identified three different equations for initiation

pressure.

- *Nonporous medium*. If $\sigma_{22} > \sigma_{33}$, the initiation pressure (p_i) for tensile axial fracturing at $\theta = 0°\ and\ 180°$ at the circumference of the borehole is:

$$p_i = 3\sigma_{33} - \sigma_{22} + \sigma_t \quad \text{(EQ 2. 2)}$$

In this case, the material is considered as a nonporous medium. It is impossible to initiate a transverse fracture.

- *Porous, nonpermeable medium.* In this case, static situation with uniform pore pressure (p_p) is considered in the porous medium in which there is pressure in the borehole without any fluid infiltration because of zero permeability. Based on Terzaghi's effective stress law, the effective stress is equal to: pore pressure subtracted from the total stress. Therefore, the pressure required to initiate an axial fracture is:

$$p_i = 3\sigma_{33} - \sigma_{22} + \sigma_t - p_p \quad \text{(EQ 2. 3)}$$

Again, it is impossible to initiate a transverse fracture.

- *Permeable medium*. According to Biot's stress–strain component, the pressure build-up of the fluid in the porous medium causes an additional pro-elastic stress component. Therefore, the initiation pressure of an axial fracture is given by:

$$p_i = \frac{3\sigma_{33} - \sigma_{22} + \sigma_t - Ap_p}{2 - A} \quad \text{(EQ 2. 4)}$$

where A is the poro-elastic constant:

$$A = \alpha_B \left(\frac{1-2\nu}{1-\nu}\right) \quad \text{(EQ 2. 5)}$$

where α_B is the Biot's poro-elastic coefficient:

$$\alpha_B = 1 - \frac{K_b}{K_g} \quad \text{(EQ 2. 6)}$$

The moduli K_b and K_g represent the bulk modulus of the solid and the modulus of the

grains, respectively.

In this case, initiation of the transverse fracture is possible, because pore pressure near the well may lead to tensile stress along the axis of the borehole. Hamison and Fairhurst (1967) presented the initiation pressure of a transverse fracture based on the tensile breakdown solution:

$$p_i^T = \frac{\sigma_{11}+\sigma_t-Ap_p}{1-A} \quad \text{(EQ 2. 7)}$$

At this pressure, only the in-situ stress σ_{11} perpendicular to the fracture is incorporated (Weijers, 1995).

2.2.1.2 Propagation of an initial microfracture. The fracture propagation approach assumes that there are randomly distributed defects or microfractures in the rock. The stress concentration at the tip of an initial microfracture results in propagation of the fracture. Modeling fracture propagation can be aided through the use of linear elastic fracture mechanics and the cohesive zone method.

- *Linear Elastic Fracture Mechanics (LEFM)*. In 1921, Griffith developed the Linear Elastic Fracture Mechanics, which is the most prevalent method of modeling the fracture propagation. The method was modified by Orowan (1952) and Irwin (1957). The following presents an overview of the method, as provided by Warpinski and Smith (1989).

Based on Griffith's observations, brittle materials have low tensile strength due to the presence of cracks. In the theory, he assumed that the cracks were elliptical in shape with a small minor axis. He identified a relationship between the work performed during the fracture propagation and the energy of the new surface created, as

$$dW = 2\gamma da \quad \text{(EQ 2. 8)}$$

where dW is the internal work, 2γ is the newly released surface energy (for two surfaces), and da is the incremental fracture length extended. Fracturing occurs once the crack tip stress reaches the critical value

$$\sigma_c = \sqrt{\frac{2E\gamma}{\pi(1-\nu^2}} \quad \text{(EQ 2. 9)}$$

Griffith's equation was modified by Orowan and Irwin in order to add to the theory energy dissipation that occurs during the plastic deformation and microcracking. Energy dissipation is calculated by quantifying the intensity of the stress singularity at the fracture tip, also known as the stress intensity factor. Stress intensity factors have three different modes: KI (opening), KII (shear direction 1), and KIII (shear direction 2). If the stress intensity factor at the tip is less than the critical value fracture toughness (K_{Ic}), the fracture is stable; otherwise, the fracture is unstable and it will propagate (Shin, 2013; Valkó & Economides, 1995)

$$K_{Ic} = \sqrt{\frac{2E\gamma_{eff}}{(1-\nu^2)}} \quad \text{(EQ 2. 10)}$$

Fracturing occurs when the stress intensity factor reaches fracture toughness (K_{Ic}),

$$K_{Ic} = K_I \quad \text{(EQ 2. 11)}$$

- *Cohesive Zone Method (CZM)*. In the LEFM method, there are some issues that have been modified in the cohesive zone method (CZM). For example, for the LEFM method the radius of the elliptical crack tip is in the range of interatomic distances, which is not a realistic assumption. In addition, the large stresses that occur at the fracture tip do not interact with the far-field stresses. Barenblatt (1962) developed the Cohesive Zone Method in which these issues were resolved, to better capture the actual physical phenomenon. In the CZM method, the crack tip is modeled as a process zone going through

damage instead of an elliptical tip, as shown in Figure 2.4 (Shin, 2013; Valkó & Economides, 1995).

2.3 Continuum-based Numerical Methods

Continuum-based methods are most commonly used to simulate hydraulic fracture processes in complex 3D geometries. The finite difference method (FDM), the finite element method (FEM), and the boundary element method (BEM) are the most popular continuum-based methods used in rock mechanics (Jing & Stephansson, 2007; Nadimi et al., 2013; Nadimi & Shahriar, 2014). Due to the continuum concept of these methods, modeling of inelastic deformation and brittle fracturing is classified as an indirect method. In addition, the damage or fracture cannot be observed by these methods. Accordingly, damage is represented by its effect on constitutive relations (Park et al., 2004; Potyondy et al., 1996). The basic assumption of these methods is that the materials are considered as continuous media throughout the physical process. Based on that assumption, the material cannot fracture or break into pieces. All material points are in the neighborhood of certain points in a simulation domain and remain in the same adjacent neighborhood throughout the simulated physical process. In the case of the presence of natural fractures in the materials, continuum-based methods assume that deformation along or across the fractures has the same order of magnitude as that of the solid matrix near the fractures. Therefore, the effect of the discontinuities is largely neglected in simulation because no large-scale macroscopic slip or opening of fractures should occur. During the last decade, some special algorithms have been developed to address the problems occurring in numerical hydraulic fracturing simulation by continuum-based methods, such as special joint elements in FEM and the displacement discontinuity technique in BEM (Jing & Stephansson, 2007). Linear

elastic fracture mechanics (LEFM) is not capable of characterizing crack initiation; therefore, it has been used to investigate the propagation of a preexisting fracture (Yang, Sheng, Ye, & Tan, 2011).

Most of the continuum-based methods used for simulating the hydraulic fracture process are not capable of characterizing crack initiation. Barrenblatt (1960) and Dugdale (1962) proposed the cohesive zone finite element method that has been widely used to simulate the fracturing process in solid materials (Barenblatt, 1962; Dugdale, 1960). In the continuum-based approach, the cohesive-zone concept modifies local continuum mechanics equations in order to deal with the discontinuities (Ha & Bobaru, 2011). The cohesive zone model assumes that the existence of a fracture process zone is characterized by a traction-separation law. The singularity of the stress field of the crack tip in classic fracture mechanics was avoided in the cohesive zone model. The cohesive zone can be easily adapted to the finite element method. Hereby, the cohesive finite element method is a quantitative analysis method for the fracturing process (Z. Chen, Bunger, Zhang, & Jeffrey, 2009).

Numerical simulations of hydraulic fracturing using continuum-based models can only be applied with the following limitations:

(1) To maintain macroscopic material continuity (a basic concept of continuum methods), large-scale slip and opening of fracture elements are prevented;

(2) The global stiffness matrix should be maintained well-posed; therefore, the number of fracture elements must be kept relatively small. In that case, the numerical stabilities should be provided;

(3) Because of the use of special algorithms, complete detachment and rotation of elements, or groups of elements, as a consequence of deformation are not allowed.

(4) These methods are sometimes time-consuming (Yang et al., 2011) .

These limitations led to the conclusion (Yang et al., 2011) that the continuum-based methods are suitable for simulation of problems with no fracture, or for problems that include undergoing only small deformations. Although special integration algorithms or constitutive models have been developed to deal with large discontinuity problems and nonlinear behavior of materials, continuum-based numerical methods are the most appropriate for simulating problems with small deformation and linear constitutive behavior. When discontinuous media problems like fractured rocks, which contain discontinuities at various scales, are simulated by continuum-based methods like FEM, it is important to formulate the constitutive models of the continua in a way that properly represents the effects of the fractures on the equivalent material properties (Jing & Stephansson, 2007).

Unfortunately, continuum models typically do not recognize the substantial discontinuity characteristics and accordingly do not allow for the identification of important sub-continuum material properties (Boutt, Cook, McPherson, & Williams, 2007). To summarize, due to the difficulty posed by modeling a fully 3D hydraulic fracture, as described herein, continuum-based numerical simulation still remains a challenging problem (Z. Chen et al., 2009). In the following section, the application of the DEM method for simulating the hydraulic fracture process is explained.

2.4 Discontinuum-based Numerical Methods

Discrete element method (DEM) is the commonly adopted numerical method for simulating discontinuous media which includes all numerical methods treating the problem domain as an assemblage of independent units. Cundall (1979) proposed DEM to study the

discontinuous mechanical behavior of rock, which is used in many other fields, such as geomaterials and concrete (Cundall & Strack, 1979; Hentz, Donzé, & Daudeville, 2004; Hunt, Meyers, & Louchnikov, 2003; S Nadimi, Shahriar, Sharifzade, & Moarefvan, 2010; Sheng, Lawrence, Briscoe, & Thornton, 2004; Yang et al., 2011). In DEM, each particle in a granular system interacts with other particles through surface contact in which the contact points are allowed to deform according to force-deformation law (Cook et al., 2004). In the DEM method, cyclic equations are calculated based on both the specified force-displacement law and Newton's second law of motion. Material particles are bonded together at contacts and may be separated when the bond force exceeds the contact strength or energy. Therefore, DEM is capable of simulating the motion of individual particles and, accordingly, the behavior of bulk material where it is formed by assembling the bonding behavior of many particles contacts based on specific constitutive laws.

In a DEM approach, contact properties, combined with the size and shape of the particles, are the most important parameters. When the applied external force exceeds the material strength, flow and separation of the particles assembly occur. Hence, bond contact disaggregation leads to damage modes in DEM simulation. One of the most significant advantages of the DEM method over a continuum-based method is the way in which DEM discretizes the material domain, solving some of the difficulties encountered by traditional methods of fracture simulation in solid materials (Yang et al., 2011).

DEM has been developed for problems with fractured rock, granular materials, and multibody systems, as well as fluid mechanics problems. For rock mechanics problems, the rock blocks are defined by intersecting the fractures whose locations, dimensions, and orientations are required for determining the geometry of the simulation. Dead-end and isolated fractures are discarded in DEM simulation because the initiation and propagation

at tips of fractures cannot be effectively simulated at the models. To represent the behavior of a real rock, a Bonded Particle Model (BPM) was proposed, in which the rock particles can be regular circular disks (2D), spherical balls (3D), or irregularly shaped solid particles (Potyondy & Cundall, 2004). BPM was also modified to couple the fluid flow throughout the material by defining a fluid flow network within the model.

Bonded Particle Modeling (BPM) in PFC2D-3D (Manual, 1995) and Discrete Fracture Network (DFN) simulation, as well as a novel smooth joint model, are well-established methods that have been developed based on Synthetic Rock Mass (SRM) samples, used to model jointed rock masses. However, the particles in the model are discretized to the domain and are not necessarily a direct representation of rock grains or blocks; they also provide appropriate mechanical behavior including crack formation from bond breakage (Fu, Johnson, & Carrigan, 2013; Manual, 1995).

DEM offers several advantages over traditional linear fracture mechanics-based simulators:

- In the DEM method, fracture propagation is not limited to occurring along a prescribed plane; in other words, a fracture can be propagated outside of a plane. Therefore, DEM is capable of simulating fracture branching and reorientation.
- Tensile and shear rock breakage can be explicitly modeled and correlated in the DEM model.
- The strain energy stored in the bonds at the moment of failure can be grouped into synthetic microseismic events. These data could be verified by the actual microseismic information (Fu et al., 2013).

The DEM approach has several advantages over the continuum-based approach;

in the DEM method, Newton's second law is used to trace the motion and interactions of individual particles rather than the complex constitutive relationships used in continuum methods. Additionally, particles interact through contacts and bonds with other particles, and fracturing occurs once the force on bonds exceeds the strength between particles. Therefore, the DEM does not require special meshing or slip surface algorithms as do continuum methods (Park et al., 2004).

Among the most notable drawbacks of DEM for a rock mechanics problem are the characteristics of discontinuities like the locations, orientations, and dimensions of the fractures, except for some major features (large faults or fracture zones, for example) that can be deterministically characterized. The effects of these parameters are largely unknown prior to the problem setup, and may remain so even after problem solution. Therefore, the problem solution contains an essentially unknown uncertainty about the fracture system geometry. This problem plays a significant role in hydraulic fracturing simulation, where a small fracture or discontinuity around the perforation hole may have a great effect on the initiation and orientation of a fracture network. Hydraulic fracturing and fluid flow simulation in fractured rock masses relies on the fracture system characterization, and therefore presents a significant degree of uncertainty

In a discrete system, the individual units (blocks) or grids are independent and move according to the applied force, not acting as continuum media. The movement of units is constrained and controlled by their boundary surfaces and other external loads according to the equations of motion. Therefore, a block's motion can be isolated from other blocks. Conversely, for the continuum methods, the individual units (elements) are kept within the same neighborhood of other grids or elements and not free to move, based on the displacement compatibility conditions due to the continuity assumption. Therefore, the

contact of an element with neighboring elements is fixed during the course of simulation and the motion of the element is restricted by other neighboring elements connected along its boundaries.

Accordingly, a continuous method best represents the whole deformation of the system, while the discrete method better represents individual unit deformation within the system. In DEM model, block deformation makes no strain inside the block but does produce displacement of blocks, often on large scale. Therefore, the complete deboning of the rigid body motion mode, as well as the continuous deformation mode of individual units, is usually adopted in DEM.

Although there are a variety of existing models to simulate hydraulic fracturing, there is still a gap between developed methods and imminent industry needs to predict the actual process of hydraulic fracture. Seismic and field studies have proven the complexity of hydraulic fracture networks and the effects of different parameters on fracture propagation (King, Haile, Shuss, & Dobkins, 2008; Warpinski & Teufel, 1987).

Computational cost is another important issue for numerical models using the explicit coupling strategy. In DEM simulation of hydraulic fracturing, for resolving multiple dynamic-physical equations, time step should be applied minimally, thus increasing the time of the simulation (Jing & Stephansson, 2007). A typical DEM simulation may include millions, even billions of particles and interactions, and in each time step of the simulation, the movement equations for all particles are solved. As a result, this method is CPU intensive and prohibitively computationally expensive (Rougier, Munjiza, & John, 2004).

In addition, DEM is considered to be a nondeformable approach in time explicit numerical schemes. It is supposed to have limited performance once stresses and

deformation of the elements are considered in a static framework (Donzé, Richefeu, & Magnier, 2009). Although the developed lattice-Boltzmann discrete element method (LBDEM) coupling is capable of capturing coupled fluid-solid behavior under some assumptions (like presenting only small amounts of the fluid present), in certain conditions, the appropriate modeling of granular porous media is not allowed by the model formulation (Boutt et al., 2007).

In this chapter, the pros and cons of some of the numerical approaches have been evaluated. Each of the approaches has its own problems in simulating a discontinuous media; in most cases, oversimplification due to these limitations is one of the most problematic elements.

This thesis evaluated the utility of a new approach, the peridynamic theory, for simulating the hydraulic fracture process. In the next chapter, the application of the peridynamic theory in different aspects is evaluated, and then it is used to simulate the hydraulic fracturing phenomena.

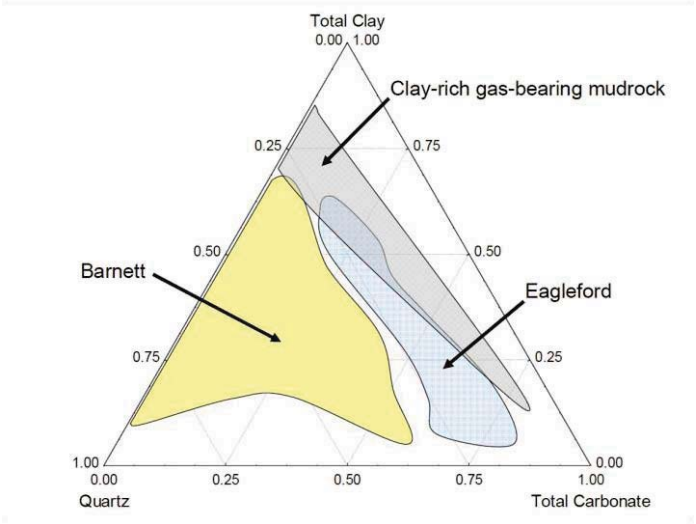

FIGURE 2. 1 Mineral composition is quite variable in each shale gas reservoir (Passey et al., 2010a)

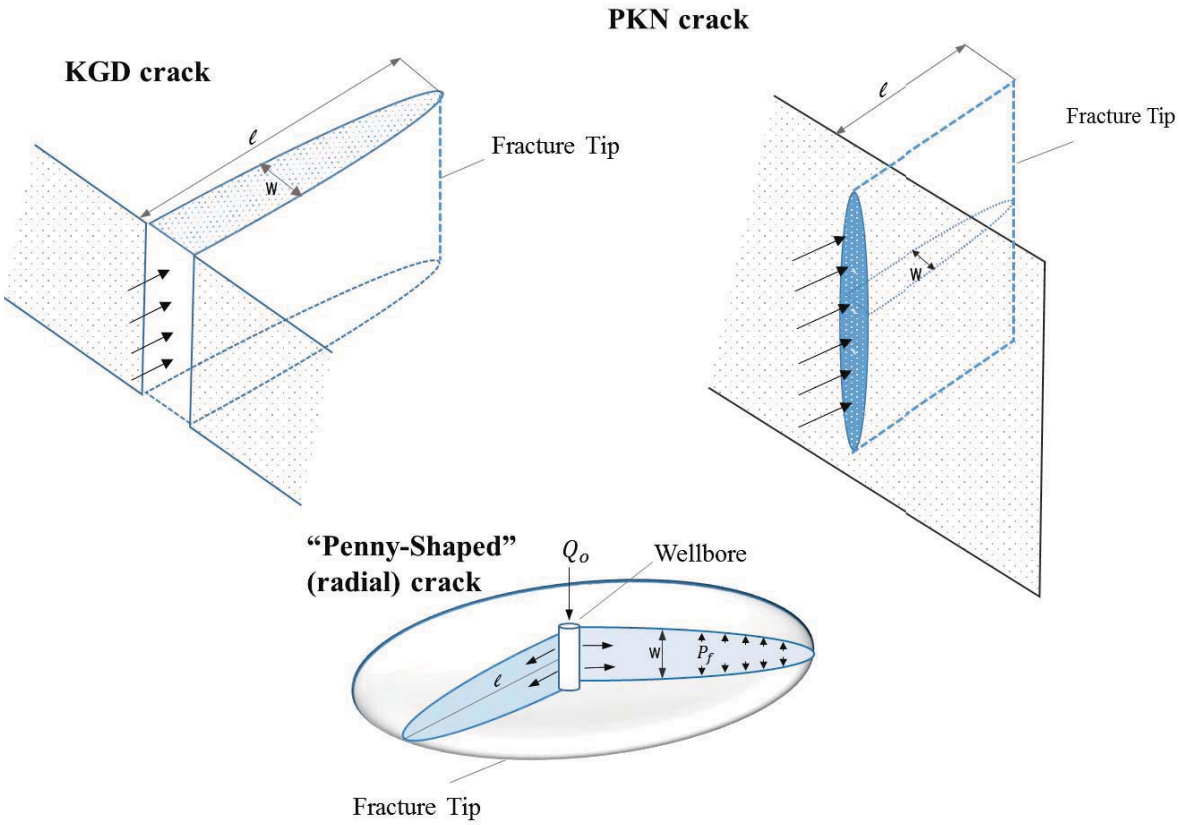

FIGURE 2. 2 Three different 2D hydraulic fracture models (KGD, PKN, and Penny-shaped)

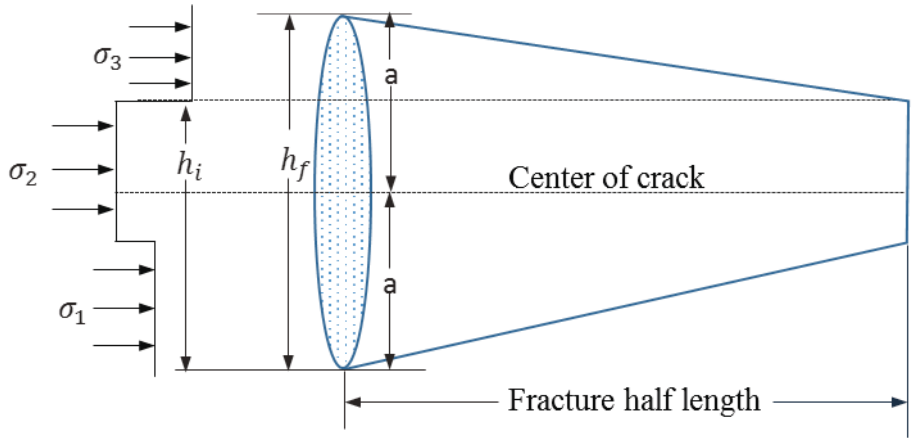

FIGURE 2. 3 Pseudo-three-dimensional (P-3D) model, after (Rahman & Rahman, 2010)

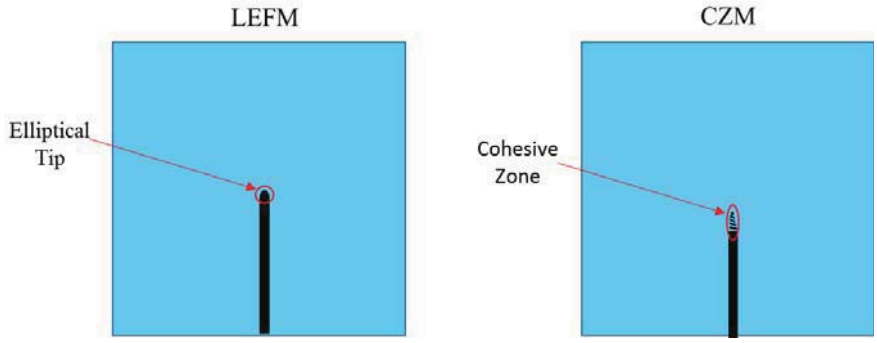

FIGURE 2. 4 . Difference between liner mechanics and cohesive zone method on crack tip modeling, after (Barenblatt, 1962)

CHAPTER 3

PERIDYNAMIC THEORY

3.1 Basics

The peridynamic theory was developed by Silling in 1998 based on the physics of a material body in which a point in the material interacts with all points within a certain distance (Silling, 1998). The proposed method is classified as a nonlocal method because particles are separated by finite distance, and they have pairwise interaction between two particles even when they are not in contact (Silling, 2000). In other words, in the local theory, material points are influenced only by the points in the immediate neighborhood, while in nonocal theory, a point is affected by points located within the "material horizon, δ", which is a region of finite radius (Figure 3.1)(Kilic & Madenci, 2009; Madenci & Oterkus, 2014; Silling, 1998). In the general peridynamics (the bond-based peridynamic), the pairwise interaction between two particles in the material horizon is called "bond" and acts like a mechanical spring in the continuum-based theory (Yu et al., 2011).

In peridynamics modeling, the particle (infinitesimally small free-body) initially obeys Newton's second law. In addition, there is a specified internal force density function between two pairs of particles that is proposed to act as if they are placed in the material horizon. However, the main difference between classical continuum theory and the peridynamic theory is that in the former, the partial differential equations are replaced by

integral equations. Since the displacement derivatives are not included in the peridynamic method, it is able to compute displacement everywhere, whether or not the discontinuouity is present (Gerstle et al., 2007; Silling & Lehoucq, 2010).

In the peridynamic theory, there are three types of numerical convergence: (a) m-convergence, in which the size of the bond remains fixed while increasing the grid density, (b) δ- convergance, in which the horizon size decreases to zero but the number of nodes inside the horizon remains the same (see Figure 3.2), and (c) δm-convergence, in which the horizon decreases with decreasing m, but where m increases equally fast or faster than δ decreases (Breitenfeld et al., 2014; W. Hu, Ha, & Bobaru, 2012).

The peridynamics equation of motion at a reference configuration of x and time t is given as (Kilic & Madenci, 2009):

$$\rho \frac{\partial^2 u}{\partial t^2} = \int_R dV_{x'} f(u(x',t), u(x,t), x', x, t) + b(x,t) \qquad \text{(EQ 3. 1)}$$

where f is the response function that point x' applies on point x; the response function is defined as the force vector per unit volume squared. ρ is the mass density, R is the neighborhood of x, dV_x is the integration variable that indicates An infinitesimal domain located at point x', u is the displacement vector field, and b is a prescribed body-force density field.

ξ is the relative location of the two particles in the reference configuration and η is their relative displacement,

$$\xi = x' - x, \qquad \eta = u(x',t) - u(x,t) \qquad \text{(EQ 3. 2)}$$

The force within a material is defined based on the interactions between the pairs of points. The movement in a point is calculated based on the summation of forces between itself and all of the points on the horizon (Kilic, 2008).

During the last decade, three different models of the peridynamic theory have been developed: bond-based, ordinary state-based, and nonordinary state-based models. In the bond-based peridynamic, the pairwise force function includes all of the constitutive information about material, except three concepts (Silling et al., 2007):

The assumption that all of the pairs of particles interact only through a central potential results in an oversimplification. For example, this oversimplification leads to fixed Poisson's ratio of ¼ in isotropic linear microscopic materials.

In continuum mechanics, the constitutive behavior of the material is described based on stress-strain tensor. Representing the material model in terms of the pairwise force function results in some difficulties in the use of the peridynamics approach. Plasticity in bond-based materials can be modeled by permitting permanent deformation of individual bonds, which is inconsistent with plastic incompressibility in metal. That is, the experimental observations show that only shear deformation can elicit a plastic response.

By introducing the rotational degree of freedom into the bond-based peridynamic model, the first problem will be solved, and in that case, it will allow modeling of materials with a Poisson ratio other than ¼. In order to solve other problems, in the state-based peridynamic, the material-dependent part of the peridynamic model was rewritten and a mathematical object called a force-state was added to the theory. This is in some ways similar to the traditional stress tensor. Therefore, it is possible to implement constitutive models in the peridynamic theory.

In an ordinary state-based theory, the force vector, T, maps a deformation-state into a force-state at all points within a volume of influence in which there is no restriction on the mapping function being linear or continuous. In this method, the bond force depends on the collective deformation of the bonds in the volume of influence, since restrictions of

the bond-based peridynamic is eliminated in this model (Breitenfeld et al., 2014).

In contrast to the ordinary state-based peridynamic, in a nonordinary state-based model, the force-vector, T, is introduced based on the strain and stress tensors. This model does not necessarily need co-linearity between the continuum points. Therefore, it allows the researcher to use the quantities of classical continuum models, such as deformation gradient and stress tensor, in constitutive models. Accordingly, this allows for the incorporation of the classical constitutive models into PD without reformulating the constitutive laws in terms of the force-factor state (Breitenfeld et al., 2014).

3.2 Response Function

Material particles interact with each other through a constitutive model associated with the material. However, the response formulation must obey the liner and angular admissibility condition that derives from Newton's third law, as:

$$f(-\eta, -\xi) = -f(\eta, \xi) \qquad \text{(EQ 3. 3)}$$

in which the relative position in a reference configuration ξ can be expressed as $\xi = x - x'$ and the relative displacement η is given as $\eta = u' - u$ as illustrated in Figure 3.3. Eq. (3.3) will be called the linear admissibility condition on f (Silling, 2000).

The response function is valid for both linear and nonlinear analysis. Based on the conditions of the modeling, different functions can be used to define the response function, as Van der Waals force was used by Silling and Bobaru to model nano-scale structure (Silling & Bobaru, 2005).

3.3 Application of PD in Heterogeneous Media

In this section, the application of peridynamic theory in heterogeneous media is evaluated and the utility of peridynamic theory for simulating the hydraulic fracturing phenomenon in unconventional reservoirs is described. Based on previous studies, it is evident that peridynamics theory is capable of modeling and simulating heterogeneous and anisotropic media.

3.3.1 Heterogeneity in Unconventional Reservoirs

Brittle and clay-mature shale gas and tight oil formations (unconventional reservoirs) are anisotropic and heterogeneous, exhibiting significant variation in strength and modulus. Tight gas shale has unconfined compressive strength ranging from 34 MPa (5000 psi) to 48 MPa (7000 psi) with Young's modulus ranging from 1×10^6 to 10×10^6. Shales are dense materials with low porosity and low permeability matrix that have intricate patterns of fracture. The fracture network in shales is mostly well mineralized, which decreases the permeability. Accordingly, these formations are actually impermeable, stiff, heterogeneous, and strongly anisotropic. Shale formations are considered as transversely isotropic materials with higher modulus direction (stiffness direction) parallel to the bedding. According to FEM and analytical modeling, the degree of nonuniformity in shale layers strongly depends on the shear modulus (Suarez-Rivera et al., 2006).

Since fractures provide flow channels in unconventional reservoirs, the characteristics of the fractures in different heterogonous layers play significant roles. Therefore, predicting the fracture network in low permeable reservoirs can assist in increasing the efficiency of the hydraulic fracturing technology as well as the production rate (Rijken & Cooke, 2001).

Research into the effects of the heterogeneity on geo-materials has revealed that heterogeneity influences the stress condition when hydraulic fractures initiate, and accordingly, affects the fracture propagation. By increasing the homogeneity value in the geo-materials, the cluster of the fractures induced by hydraulic fracturing decreases significantly. In addition, the hydraulic fractures propagate more symmetrically in more homogeneous geo-materials (Wang et al., 2009).

3.3.2 Application of PD in Heterogeneous Media

The peridynamic theory was initially applied to homogeneous materials, and then expanded for heterogeneous problems. Composite materials, especially those formed by reinforcing fibers in matrix materials, are heterogeneous and anisotropic. The materials exhibit high stiffness and tensile strength within the ply parallel to the fiber direction, and to a lesser extent, in compression. The primary advantage of the PD model over other numerical methods is that the same equation of motion is used to deal with the behavior of a heterogeneous medium, regardless of any discontinuities (Xu, Askari, Weckner, & Silling, 2008).

In order to introduce the anisotropy of the composite into the definition of the bonds in classic laminate theory, the concept of transverse modulus was developed. In this type of PD, three kinds of damage in composite material were analyzed: fiber fracture, matrix fracture, and delamination. The progressive damage and fracture models of laminates with unidirectional and multidirectional fiber layup were successfully simulated by PD under tensile load (Hu et al., 2014).

3.3.3 Constitutive Micropolar Peridynamics Model for Concrete

Grestle and Sau (2007) developed a micro-elastic model for concrete based on the peridynamic model with stiffness c and cut-off stretch s^*. In the aforementioned study, Grestle modified the model to investigate both the tension and compression behavior of the concrete more accurately. This model is still capable of modeling concrete only under monotonic deformation. In addition, due to the small deformations, particle rotation is neglected. Material rate-dependency is also ignored in this model. The most important consideration in this model is computational efficiency.

In the model, the pairwise force function between particles "i" and "j" depends on both the axial stretch, s, of a link between particles "i" and "j", and maximum stretch, s_{max}, of any other peridynamics links. As shown in Figure 3.4, the material behaves elastically as long as the stretch, s, remains between the tensile and compressive stretch limits (s_t, s_c). As the stretch exceeds the tensile stretch limit, the force will be reduced to β times of the former value which will remain constant until it exceeds another specific limit, $\alpha_t s_t$, after which the force will approach zero. In addition, if s exceeds the compressive stretch limit, two possibilities exist: (1) if the $s_{max} > s_t$ (connected to either particle "i" or particle "j"), the link remains linear elastic, but (2) if $s_{max} < s_t$, the compressive pairwise force remains constant until it reaches another specific limit, $\alpha_c s_c$, after which it drops to zero (Gerstle et al., 2007a).

The micropolar model proposed by Gerstle et al. for concrete has eight parameters: c, d, δ, s_t, s_c, α_t, α_c, and β. The micro-elastic parameters, c and d, are directly derived from the classical elastic parameters, Young's modulus (E) and Poisson's ratio (ν). The material horizon, δ, which is considered to be a discretization parameter, is defined based

on the size of particles. s_t and c are both related to the uniaxial tensile strength, f_t . Both s_c and c are related to the compressive strength, f_c. α_t and β are used to measure the fracture energy, G_f. α_c can be used to introduce the uniaxial compressive energy absorption capacity of concrete.

3.3.4 Laminate Modeling

Fiber reinforced composite laminate is composed of different piles with different orientations and distinct properties, which cause the material heterogeneous and anisotropic nature. Hence, it is necessary to find different micromoduli of bonds for describing the anisotropic behavior of composites. According to the model, the bonds whose orientation is parallel with that of the fibers provide the longitudinal stiffness. However, bonds with any other directions contribute to the transverse stiffness (Figure 3.5). In addition, based on the in-plane and interlayer longitudinal bonds, they are named fiber bonds (matrix bonds) and longitudinal interlayer bonds (transverse interlayer), respectively.

The micromodulus of the longitudinal bonds is defined as,

$$C_{longitudinal} = e^{-(|\xi|/\delta)} \frac{Q_L}{Q_{11}} \overline{C}_L , \quad Q_L = \begin{cases} Q_{11} & in-plane\ bonds \\ Q_{layer} & interplayer\ bonds \end{cases} \qquad \text{(EQ 3.4)}$$

and the micromodulus of the transverse bonds is defined as,

$$C_{transverse} = e^{-(|\xi|/\delta)} \frac{Q_T}{Q_{22}} \overline{C}_T , \quad Q_T = \begin{cases} \overline{Q}_\alpha & in-plane\ bonds \\ Q_{layer} & interplayer\ bonds \end{cases} \qquad \text{(EQ 3. 5)}$$

where Q_{11} and $Q_{22}$are the stiffness of unidirectional lamina in the longitudinal and transverse direction, Q_{layer} is the stiffness on interlayer (matrix stiffness), and $\overline{Q}_\alpha$is the transverse stiffness. $\overline{C}_L$ and $\overline{C}_T$ are the longitudinal and transverse micromoduli of a bond

when a homogeneous strain is applied on the unidirectional laminate along fiber direction, and unidirectional laminate transverse to the fiber direction, respectively (Hu et al., 2014).

3.3.5.1 Critical stretch of bond. The fiber-reinforced composite has a distinct strength in different directions. Hence, critical bond stretch, s_0, will be set to different values. Figure 3.6 shows the bond stretches in three different materials, in which the matrix and interlayer bonds were assumed to remain in half performance after their stretch exceeds the compressive critical value. For imposing the fracture of bonds, a time-dependent damage function was introduced to the model:

$$\mu(\xi, t) = \begin{cases} 1 & if\ s(\acute{t}, \xi) < s_0 \quad \acute{t} \in (0, t) \\ 0 & otherwise \end{cases} \qquad \text{(EQ 3. 6)}$$

where s_0 is the critical stretch value. As shown in Figure 3.6, different materials in the laminate have different critical stretch values ($s_0^{fc}\ and\ s_0^{fmc}$).

3.3.5.2 Damage definition. In the fiber-reinforced composite, the damage is categorized into three types, based on the bond types: fiber region R_{fiber}, matrix region R_{matrix} and interlayer region $R_{interlayer}$. The interlayer region can also be divided into two parts: the upper and the lower region. Hence, the damage in the subregion is expressed as:

$$R_{Subregion} = R_{fiber} + R_{matrix} + R_{interlayer_{upper}} + R_{interlayer\_lover} \qquad \text{(EQ 3. 7)}$$

Three models of damage are analyzed:

$$\emptyset_i = 1 - \frac{\sum_{nodes\ \in R_i} \mu(\xi, t)}{N_i} \qquad \text{(EQ 3. 8)}$$

where $i = fiber, matrix, interlayer_{upper} and\ interlayer\_lower$, N_i is the number of bonds in region R_i (Hu et al., 2014).

A multiscale analysis method was used in the PD laminate composite models to recognize both the macroscopic and microscopic dynamics inside the material. Nguetseng and Allaire developed the concept of the two-scale convergence (Alali & Lipton, 2012; Allaire, 1992; Nguetseng, 1989).

3.4 PD Theory for Thermomechanical Analysis

Over the last couple of years, the peridynamic theory has been used for analyzing thermomechanical problems. Research carried out in this field indicates that the peridynamic approach is suitable to be used in thermomechanical analysis of reservoir simulations. Section 3.4.1 Effects of Temperature describes the application of the peridynamic theory in thermal simulations.

3.4.1 Effects of Temperature

Formation permeability depends on several parameters like mineral dissolution/precipitation, stress condition, fluid injection/extraction, and rock temperature. Very deep formations have considerably higher temperatures than the ambient, which generally affects rock behavior as well as permeability. The stress induced by the thermal process causes fracture openings and slip along a fracture (Ghassemi, Tarasovs, & Cheng, 2007). Therefore, the effects of thermal stress on hydraulic fracturing initiation and stress measurements were investigated by several researchers.

It is important to understand the effects of the thermal environment on the fracturing fluid viscosity fracture, propant settling rates, solid blocking agent performances, acid retarder requirements, and acid reaction rates (Whitsitt & Dysart, 1970). The numerical coupling of mechanical, hydraulic, and thermal phenomenon is important in modeling

hydraulic fracturing simulation in petroleum production (Bower & Zyvoloski, 1997). According to the Howard, Fast, and Carter theory, the fracture extends in the direction opposite of the heat flow. Le Guen et al. employed pulse-decay methods to measure permeability of rock salt under thermo-mechanical stress (Le Guen, Deveughele, Billiotte, & Brulhet, 1993). Studies examining wellbore stability show that coupling between temperature and salinity has a significant influence on rock stability (Ghassemi & Diek, 2002; Zhou & Ghassemi, 2009).

Kilic and Madenci (2010) extended the PD theory to investigate the effects of thermomechanical loading. As a result, a new response function was developed to express the known material properties of bulk moduli and the coefficient of thermal expansion. The developed response function is given as:

$$f(\eta,\xi) = \frac{\xi+\eta}{|\xi+\eta|}\mu(\xi,t)\frac{9k}{\pi l^4}e^{-\left(|\xi|/l\right)^2}(s-\alpha\theta) \qquad \text{(EQ 3. 9)}$$

where θ is the temperature difference between instanteous and reference temperature between material particles x' and x, and α is the coefficient of thermal expansion. $c_1$and c_2 are the material constant. l is the internal length parameter distinguishing the different length scales. S is the stretch happening between material particles x' and x, K is the bulk modulus, and μ is a history-dependent scalar-valued function that it can be introduced as (Kilic & Madenci, 2010):

$$\mu(\xi,t) = \begin{cases} 1, & if\ s(t',\xi) - \alpha\theta < s_0 \qquad for\ all\ 0 < t' < t \\ 0, & otherwise \end{cases} \qquad \text{(EQ 3. 10)}$$

in which s_0 is the critical stretch for failure to occur.

The aforementioned method was used to investigate the effect of the heating on crack propagation by simulating a homogenous plate subjected to a temperature gradient.

The study demonstrated the ability of PD theory to predict the crack path propagation under temperature loading. The simulation shows that the PD theory successfully analyzed the curvilinear growth in the plate. In order to investigate the method's capability, two bonded dissimilar plates were considered. In the case study, the plates were free of any displacement restrictions and were exposed to a uniform temperature. The study confirmed that PD theory is capable of simulating and predicting 3D crack growth (Kilic & Madenci, 2010).

A generalized PD heat transfer equation was formulated based on the Lagrangian formulation, in which the PD heat conduction quantities are related to the quantities from the classical theory. In addition, the fully PD thermomechanical equations were derived based on the concepts of material thermodynamics. A nondimensional form of the coupled thermomechanical PD equation was presented as well. The presented heat conduction model is a continuum model that does not explicitly contain the detail of heat energy carrier motion. In the framework of PD, heat conduction is based on the interaction between material particles that exchange heat energy. The peridynamics framework was modified to include heat diffusion and thermo-mechanical coupling (Agwai, Guven, & Madenci, 2012).

3.4.2 PD Theory for Thermal Field

In the peridynamic theory, interaction among material particles is nonlocal, since heat diffusion in this method occurs between material particles based on the exchange of heat energy. In such case, heat exchanges energy between points that are located on the same horizon. The heat diffusion equation at a reference position x and time t is expressed as (Agwai et al., 2012):

$$\rho c_v \frac{\partial T(x,t)}{\partial t} = \int_H dV_{x'} f_q(T(x,t), T'(x',t), x, x', t) + \rho \bar{s}(x,t) \qquad \text{(EQ 3. 11)}$$

where c_v is the specific heat capacity, T is the temperature vector field, $\bar{s}$ is the heat source term, and f_q is a thermal response function (heat energy per unit volume squared). The material points interact with each other based on the response function. Bobaru (2010) introduced a pairwise thermal response function for isotropic materials (Bobaru & Duangpanya, 2010):

$$f_q(T, T', x, x', t) = k_q \frac{\tau(x,x',t)}{|\xi|} \qquad \text{(EQ 3. 12)}$$

where k_q is introduced in terms of conductivity (k) and the horizon radius (δ) as $k_q = 2k/(A\delta^2)$ for 1-D , $k_q = 6k/(h\pi\delta^3)$ for 2D and $k_q = 6k/(h\delta^4)$ in which h is the thickness of the volume associated with the material point x'. The relative temperature is defined as $\tau = T' - T$ (Agwai et al., 2012; Oterkus, Madenci, & Agwai, 2014). The value of the k_q depends on the domain of the integration defined by the horizon. Therefore, the value of the k_q should be corrected if the material point is close to the free surface or material interface.

3.5 Fluid Transport

Fracture propagation in a rock formation due to the hydraulic loading depends on fluid flow in the formation. There are numerous different aspects that affect fluid flow in porous media. Section 3.5.1 evaluates the simulation of fluid flow through a crack and the application of peridynamic theory in this field.

3.5.1 Fluid Flow in Rock

Fluid flow through porous media is influenced by different factors, including fluid properties as well as the mineralogical, textural, and geomechanical properties of the formation (Baca, Arnett, & Langford, 1984; Narasimhan, 1982; Oliver & Bons, 2001). Numerical and theoretical approaches have been used to study various aspects of fluid flow, such as far-field and local stress conditions and fracture interconnectivity (Holyland & Ojala, 1997; Jiang, Oliver, Barr, Power, & Ord, 1997; Matthäi & Roberts, 1997; Oliver, Ord, Valenta, & Upton, 2001). Extensive alteration of the wall rock depends on the fluid composition relative to the wall rock composition, permeability and pressure, and duration of injection (Oliver & Bons, 2001; Phillips, 1991).

The flow of fluids in many porous media is supposed to happen either in a network of closed conduits or around solid particles forming a spatial array (Dullien, 1991). The characterization of the fluid transport properties of rock has significant importance in reservoir production. Although the active seismic method has some fundamental problems (Shapiro & Müller, 1999), it is one of the most useful approaches for predicting reservoir permeability. Shapiro et al. (2002) developed a seismic-based approach to investigate permeability on the large spatial scale. Hence, the seismicity-based reservoir characterization (SBRC) technique was developed to study permeability distribution in three dimensional heterogeneous media (Shapiro et al., 2002). Fluid transport in shale and the effects of hydraulic fracturing on the permeability of the shale reservoirs have great importance in production rate (Revil & Leroy, 2004).

A coupled thermal-hydraulic-mechanical (THM) process under a multiphase flow is widespread in a number of geomechanics applications. Rutqvist et al. linked two jointly executed computer codes, TOUGH2 and FLAC3D, in order to conduct a coupled THM

analysis. The authors studied the deformation, heat transfer, and multiphase fluid flow in the fractured and porous rock (Rutqvist et al., 2002).

In classical theories of transport phenomenon like Darcy's law, Hick's law, and Fourier's law, constitutive equations were utilized to model the convection and diffusion of the fluid flux proportional to the gradient of potential. Gaussian Probability distribution function was used in these models to describe the diffusion process through the constitutive equation. However, the observation of the diffusion process in various material like polymer, biomaterial, and geological media shows that it does not follow Gaussian statistics. Actually, the geological and hydrology fields can be controlled by a strong non-locality, termed "scale-dependent dispersion." Different permeability causes fluctuations in a trace particle's velocity which leads to perplex diffusion in the formation. Other causes that can be observed in petroleum reservoirs are fracture and stress conditions, whereby the pathway of flow and the tracer's velocity are affected.

Accordingly, the PD formulation, which is a nonlocal model, is used for advection/diffusion of fluid in porous media. Bobaru (2010) and Dangpanya (2012) developed the PD for diffusion and formulated a peridynamics model for isotropic transient heat conduction (Bobaru & Duangpanya, 2010, 2012). The PD formulation was extended to model the advection/diffusion (Du, Gunzburger, Lehoucq, & Zhou, 2012; Du, Kamm, Lehoucq, & Parks, 2012). Katiyar et al. (2014) developed a state-based PD formulation to model the conductivity of a single-phase flow of a liquid with small and constant compressibility in a heterogeneous porous media. In addition, a bond-based PD formulation was developed and demonstrated as a special case of the state-based formulation. The model presented the arbitrary flow in discontinuities/heterogeneous porous media without any fundamental changes to the model. Accordingly, the Bobaru and

Dangpanya model was generalized to anisotropic diffusion in heterogeneous materials with application to fluid porous media (Katiyar, Foster, Ouchi, & Sharma, 2014).

3.5.2 State-Based PD Formulation of Single-Phase of a Liquid with Small and Constant Compressibility through Porous Media

A general state-based peridynamic model was presented by Katiyar et al. (2014) for convective single-phase flow of a liquid of small and constant compressibility in porous media. In the model, the possible anomalous diffusion due to nonlocal fluid flow was considered. To develop a governing equation based on PD for modeling the flow in porous media, an analogy was sought in the quadratic function of the vibrational form of the mass conservation equation using the classical continuum mechanics theory. The mass conservation equation for single-phase fluid flow in porous medium at position x and time t, using classical theory, is

$$\frac{\partial}{\partial t}(\rho[x,t]\phi[x,t]) = -\nabla.(\rho[x,t]u[x,t]) + R[x,t] \qquad \text{(EQ 3. 13)}$$

where u is the volumetric rate of mass flow per unit bulk cross-sectional area, ρ is the fluid density, $\emptyset$ is the medium porosity, R is the mass generation per unit bulk volume per unit time, and $\nabla.$ is the standard divergence operator. The volumetric flux of fluid can be defined based on Darcy's law for laminar flow as,

$$u[x] = -\frac{1}{\mu}K[x]\nabla\phi[x] \qquad \text{(EQ 3. 14)}$$

where K is the tensorial form of the permeability of the porous medium and μ is the fluid viscosity. The flow potential in terms of fluid pressure p[x] is,

$$\phi[x] = p[x] + g\rho[x]z[x] \qquad \text{(EQ 3. 15)}$$

where z and g are the spatial coordinates in the upward direction and gravitational acceleration, respectively (Katiyar et al., 2014). The presented formulation is general for

fluid mass flow through any arbitrary bonded body that relates mass flow state with the flow potential state. In the study, a constructive model was used in which the flow in a bond only depends on the potential difference in that bond. In the model, the nonlocal constitutive parameters were represented in terms of the material properties.

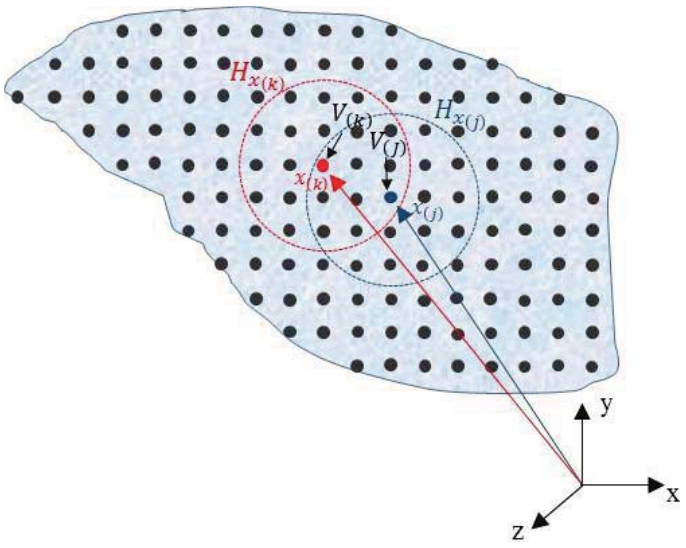

FIGURE 3. 1 Infinitely many PD material points and interaction of points at x_k and x_j, after (Madenci & Oterkus, 2014)

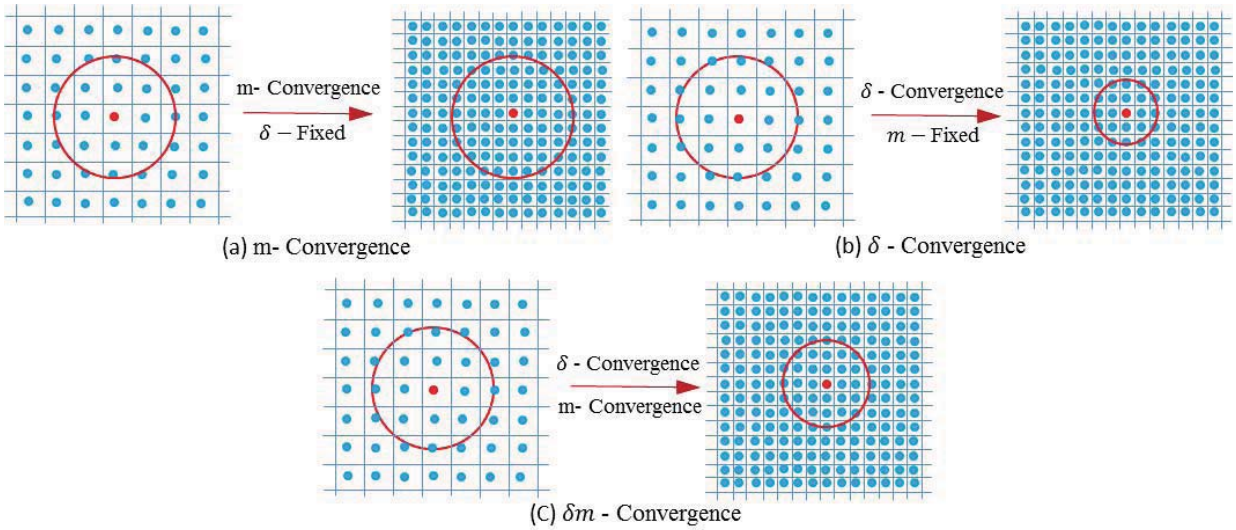

FIGURE 3. 2 Two types of numerical convergence: (a) m- convergence (b) δ-convergence, after (Silling et al., 2007)

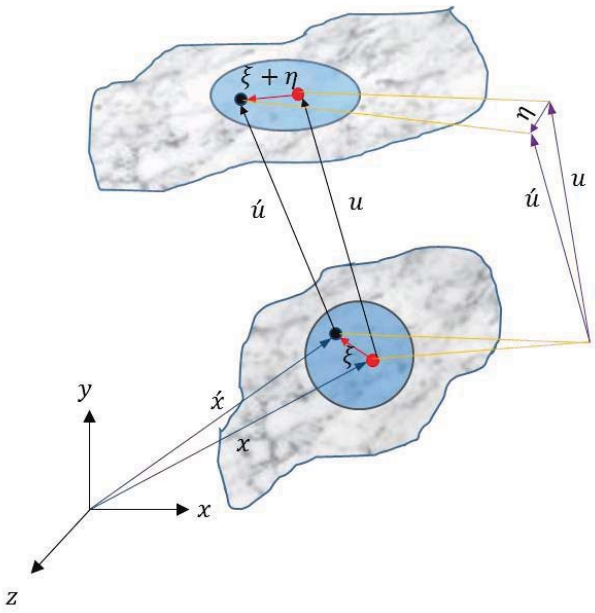

FIGURE 3. 3 The position of two material points in the initial and deformed states, after (Sakhavand, 2011)

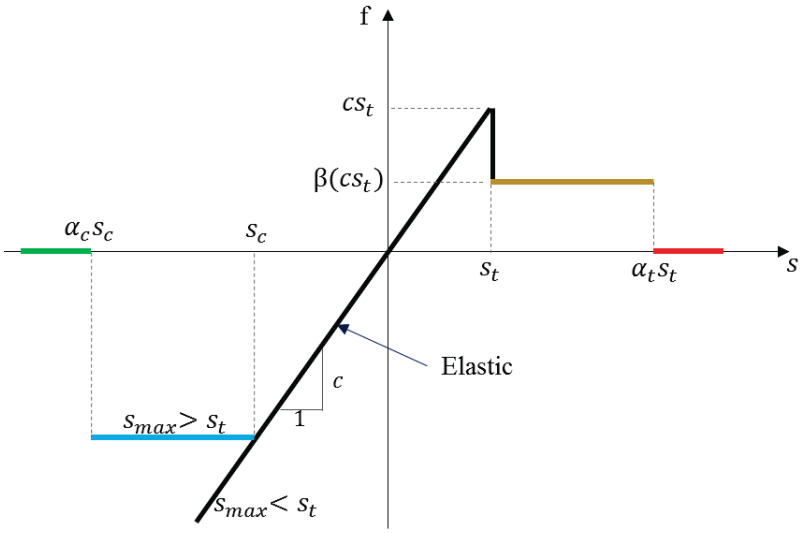

FIGURE 3. 4 Micropolar constitutive model for concrete, after (Gerstle et al., 2007b)

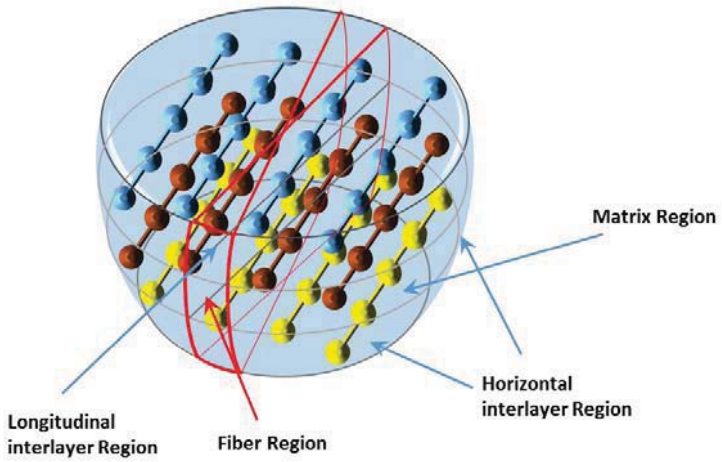

FIGURE 3. 5 Partition of fiber matrix, and interlayer region, after (Yu & Wang, 2014)

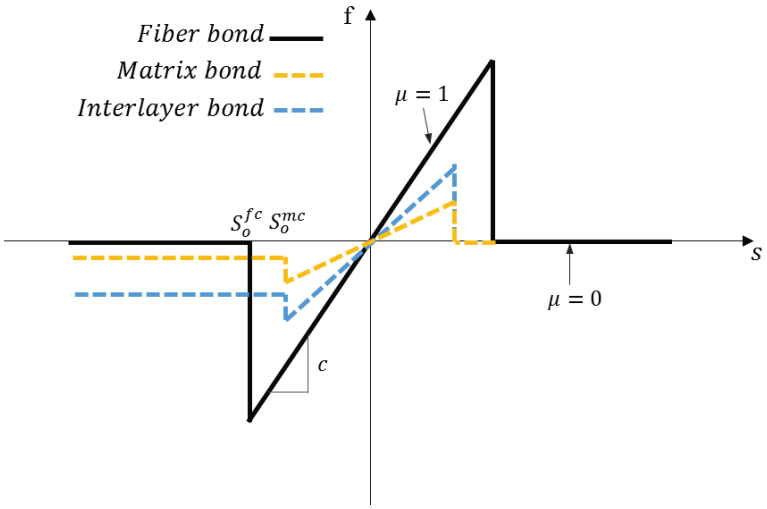

FIGURE 3. 6 Relationship between bond and pairwise force function f of bonds, after (Yu & Wang, 2014)

CHAPTER 4

NUMERICAL IMPLEMENTATION AND MODEL VALIDATION

4.1 Hydraulic Fracturing Models

Hydraulic fracturing in unconventional reservoirs often results in a complex-fracture network that requires optimization of the stimulation design and completion plan (Fisher et al., 2005; Le Calvez et al., 2007). Hence, the modeling of fracture initiation and propagation is essential for optimization. Unfortunately, most of the common hydraulic fracture models in the industry are not able to properly simulate complex fracture networks. One of the most important general hydraulic fracture models that incorporates a full coupled hydro-mechanical model was developed by Zhang et al., but is a 2D plain-strain model that is applicable for situations in which fracture length is much greater than the height (Zhang, Thiercelin, & Jeffrey, 2007). A complex fracture-network model that is capable of predicting the fracture propagation and the interaction with preexisting natural joints and fractures was presented by Olson (Olson, 2008). However, the model only contains fracture mechanical aspects and does not include fluid flow and propant transport. Weng et al. (2011) presented a model that simulates the complex propagation of fractures in a heterogeneous formation. The model includes a solution for fracture deformation, height growth, fluid flow, and propant transport in a complex fracture network (Weng, Kresse, Cohen, Wu, & Gu, 2011).

4.2 Application of Peridynamics in Hydraulic Fracturing

Within the context of hydraulic fracturing, it is important to model the interaction between porous media and fluid flow and the effects of the fluid on the interstitial surface. To model this interaction, Turner (2013) used the modified nonlocal peridynamics model (state-based peridynamics) on the base of fluid pore pressure. The study simulated the influence of the fluid pore pressure by effective stress, as developed by Terzaghi and Biot (Biot, 1941; Biot, 1955; Terzaghi, 1943). The state-based peridynamic approach is capable of forming a constitutive model from the conventional theory of solid mechanics and can compute the material behavior based on collective quantities such as a volume change or a shear angle, making the approach suitable for the modeling of saturated porous media. The effective stress principle is representative of a new peridynamics material— a saturated porous medium effectively loaded by the fluid pressure in the pores. According to Turner's study, the direct influence of the fluid has not been represented, only its effects (as effective stress) on the constitutive behavior of the porous medium. Hence, it is important to recognize that in the material influenced by pore pressure, the effective stress principle does not change the constitutive behavior (Turner, 2013).

The theory of interacting continua was used to form the interaction force between pore fluid and the solid matrix surface. In this formulation, the effect of the interaction was presented as a volumetric change. To present this model, the ordinary linear elastic peridynamic was used in the first stage, then the behavior of the material changed in the peridynamic representation. Therefore, for presenting this material based on the standard linear elastic peridynamics material, the force scalar state was split into (1) the dilatational or volume changing term and (2) the deviatoric term. Modeling of the interaction between fluid and solid is highly complex and only a simple case of a drag-like term was considered.

For validating the formulation and understanding the influence of the effective fluid pressure, several simulations were carried out in which a particular fluid pressure was applied (Turner, 2013).

The simulation of hydraulic fracturing was performed on a three-dimensional domain with a thickness of 0.5 cm, assuming plane strain. If the pore fluid pressure is large enough, it will lead to an increase of stress in the porous media and cause fractures in the media. The extension of the induced fracture depends on the properties of the fluid and the injection rate. The influence of the leak-off test on the porous media was evaluated by dilation of a borehole with displacement at various depths of fluid penetration. Displacement near the borehole was significantly increased because of the leak-off effects, but the influence did not propagate deeply in the initial penetration. Then, the displacement in depth increased as the fluid depth increased. The presented formulation is well suited for evaluating the influence of the leak-off process (Turner, 2013).

4.3 Model Validation

In this thesis, the experimental study done by Zhou et al. (2008) was used to validate the numerical simulation of hydraulic fracturing by the peridynamic theory. In this study, the hydraulic fracture phenomena were studied through a series of laboratory tests. The influence of the angle of approach, differential horizontal stress, and shear strength of preexisting fracture on the fracture propagation behavior was investigated through the experimental tests. The fracture geometry and propagation path was mainly controlled by preexisting fracture and in-situ stress regime.

4.3.1 Shear Slippage

Shown in Figure 4.1, a single preexisting fracture intersects with hydraulic induced fracture, parallel to the direction of maximum horizontal stress σ_v, with an angle of θ from σ_H. The lack of sufficient normal stress on the fracture planes is the main reason for shear slippage. The linear friction relationship between the normal and shear stress acting on a natural fracture plane is presented as

$$|\tau| = \tau_0 + K_f(\sigma_n - p) \quad \text{(EQ 4. 1)}$$

where τ is the shear stress, τ_0 is the inherent shear strength of the natural fracture plane, K_f is the coefficient of friction, σ_n is the normal stress, and p is the pore pressure. In this relationship, the shear slippage occurs on the fracture plane if:

$$|\tau| > \tau_0 + K_f(\sigma_n - p) \quad \text{(EQ 4. 2)}$$

Based on the 2D stress solution, the shear and normal stresses acting on the fracture plane can be found as

$$\tau = \frac{\sigma_H - \sigma_h}{2} sin\, 2(90 - \theta) \quad \text{(EQ 4. 3)}$$

and

$$\sigma_n = \frac{\sigma_H + \sigma_h}{2} + \frac{\sigma_H - \sigma_h}{2} cos\, 2(90 - \theta) \quad \text{(EQ 4. 4)}$$

When the hydraulic fracture is blunted at the interface, the pore pressure at the intersection is given:

$$p = \sigma_3 + p_\sigma \quad \text{(EQ 4. 5)}$$

where p_σ is the treatment pressure. Due to the blunted crack tip, the stress singularity will have diminished and small stress components will be generated at the interaction. The criterion can be mathematically developed for the shear slippage. Therefore, by substituting Equations (4-3) and (4-5) into Equation (4-2):

$$(\sigma_H - \sigma_h) = \frac{2\tau_0 - 2p_\sigma K_f}{\sin 2\theta + K_f \cos 2\theta - K_f} \quad \text{(EQ 4. 6)}$$

and for natural fracture dilation as

$$p > \sigma_n \quad \text{(EQ 4. 7)}$$

substituting Equations (4-3) and (4-4) in Equation (4-7), we find the dilation will occur when

$$p_\sigma > \frac{(\sigma_H - \sigma_h)(1 - \cos 2\theta)}{2} \quad \text{(EQ 4. 8)}$$

Therefore, leak-off will be enhanced by shear slippage and it may cause some offset in fracture growth. Dilation will lead to formulation of multiple fractures.

4.3.2 Laboratory Hydraulic Fracturing Experiments

Hydraulic fracturing tests were conducted in a true tri-axial pressure machine. In the study, cubic blocks with a dimension of 30 cm on each side were used to perform hydraulic fracturing tests (Figure 4.2). The specimens were made from a mixture of Chinese cement no. 325 and fine sand. To prevent building shear stress along the plates, the sides of the blocks were covered with thin Teflon sheets and Vaseline. A servo hydraulic pump of MTS 618 provided the hydraulic fluid injection.

A central hole with a 0.6 cm diameter was drilled to a depth of 14 cm parallel to the sides of the block. Then a steel tube 13 cm in length was epoxied to the hole, leaving a 1 cm opening at the bottom hole section. The fractures propagated through the block and interacted with a single preexisting fracture at a certain approach angle (θ). To build a preexisting fracture, three different types of paper of different thicknesses were cast into each block. The angles between the preexisting fracture and the hydraulic fracture, θ, which varied symmetrically, were 30°, 60°, and 90° (Figure 4.3). The flow rate for the

fracturing fluid was about 4.2×10^{-9} m^3/min.

As the experiments were completed, the blocks were cut to investigate the hydraulic fracture geometry and path. Based on the different experimental conditions, the propagation direction of the hydraulic fracture before and after interacting with the pre-fracture was evaluated. The rock mechanical parameters of the block are shown in Table 4.1.

The tests were conducted in a normal-faulting stress regime in which the maximum stress was vertical with a constant value of 20 MPa; meanwhile, the horizontal stresses were changed from 3 to 10 MPa. Therefore, the influence of approaching angles and horizontal stress differences on the hydraulic fracture propagation was investigated. A summary of experimental conditions and results of the hydraulic fracture tests are illustrated in Table 4.2.

Guar gum fracturing fluid was used to apply hydraulic pressure with the viscosity of 135 MPa. The preexisting fracture was created by a sheet of printer paper with thickness of 0.11mm. Direct shear tests were conducted to determine the toughness of the preexisting fracture. In the study, the coefficient of friction for the second type of the tests was 0.89.

4.3.3 Experimental Results

The influence of different approach angles and horizontal stress conditions on hydraulic fracture was evaluated in a series of laboratory tests. A summary of these experimental tests and results of hydraulic fracture tests are presented in Table 4.2. Depending on the different experimental conditions, in some cases, the hydraulic fractures crossed the preexisting fracture, whereas in others, the hydraulic fractures were arrested by the preexisting fracture. Additionally, in some of the tests, the hydraulic fracture led to

dilation of the preexisting fracture as induced by fluid flow along the fracture surface. Therefore, based on the aforementioned behaviors, the experimental results are classified into three categories: Crossed, Dilated, and Arrested.

In Figure 4.4, the different types of fracture propagation behaviors are presented as dependent on the differential horizontal stress and the angle of approach. The results show that the hydraulic fracture crossed the preexisting fracture only at the high differential stress and approach angle of 60° or greater. On the other hand, in the lower differential stress and approach angle, the hydraulic fracture was arrested by or caused dilation of the preexisting fracture. These results are consistent with experimental results achieved by Blanton (1986) and Warpinski and Teufel (1987). For example, in their experimental study, hydraulic fracture crossed the preexisting fracture at the 60° approach angle and 7 MPa horizontal differential stress (Blanton, 1986; Warpinski & Teufel, 1987).

4.3.4 Simulating the Experimental Tests and Validating the Model

The validity of the peridynamic simulation was established by comparing it against the experimental results explained in Section 4.3.3. In the case of the validation, six sets of hydraulic fracture tests were simulated and the results compared with the experimental results. PDLAMMPS open source software was used to simulate the hydraulic fracturing process. Therefore, a lattice-based viscoelastic peridynamic simulation was established to simulate the experiments. In this model, viscous is added to deviatoric deformation and the bulk behavior remains elastic. The lattice is simply a set of points in the domain of simulation, which is determined by a unit cell with specific dimensions. The material parameters were implemented into the model based on Table 4.1. λ is a material-dependent parameter varying from zero to one. When λ is close to one, the material obeys the Maxwell

model, whereas if λ is close to zero, it shows nearly elastic behavior. In this study, different λ values were used in order to find the proper value.

The mass density of a lattice cell is 2300 kg/m^3 and the horizon, δ, is three times of the lattice spacing. The applied stress on the injector hole was about 6.5 MPa. The parameters of the simulation are explained in Table 4.3. The simulation was performed in constant volume and energy integration to update the position and velocity for atoms in the group per each time-step. The velocity and position of each of the particles was calculated based on the velocity-velert time integration algorithm.

As shown in Figure 4.5, the results of the simulations were visualized by VisIt software. VisIt is an open source visualization tool used for generating the simulation results through time-steps and manipulating the results with a variety of operators and mathematical expressions. VizIt allows the user to save the resulting images, animations, and outputs of the simulation in several formats in order to use in a presentation or other software.

The simulation result of test 2-4, with horizontal stresses of 3 and 10 MPa and the approach angle of 60°, is presented in Figure 4.5(a) in which the hydraulic fracture crossed the preexisting fracture. The result of the simulation added to the test results (red rectangular in crossed section) is perfectly consistent with experimental results. Figure 4.5 (b) presents the results of simulation of experimental test 4-6 under the condition of 3 and 13 MPa horizontal stresses and the approach angle of 60°. In this simulation, the hydraulic fracture crossed the preexisting fracture, matching the result of the experimental tests. In Figure 4.5(c), the simulation result of the laboratory test done by Blanton is reported. With the boundary condition of $\sigma_H = 15MPa$ and $\sigma_h = 0$ MPa, the hydraulic fracture crossed

the preexisting fracture, showing strong agreement with experimental results. At higher approach angles and differential stresses, the applied normal stress on the preexisting fracture surface was high enough; hence, the initial condition prevented the shear failure of the fracture. Accordingly, the hydraulic fracture most likely crossed the preexisting fracture.

Figure 4.5(d) presents the simulation results of a test with the approach angle of 45° and horizontal stresses of 8 and 5 MPa, having a test condition in the range of tests 2-8 and 2-5. As shown in Figure 4.5(d), this was located in the dilated section (red triangular) and had good correlation with the experimental results. In the test cases with lower approach angles and differential stresses, the normal stress acting on the surfaces of the preexisting fracture was close to minimum horizontal stress, where the surfaces of the preexisting fracture slip, and shear failure occurs. Therefore, opening an induced fracture along the original direction of hydraulic fracture was difficult, and it did not cross the preexisting fracture.

In Figure 4.5(e), the hydraulic fracture was arrested by the preexisting fracture. In this test, the boundary stresses were: $\sigma_v = 20MPa$, $\sigma_H = 8MPa$, and $\sigma_h = 5MPa$, which was located in the arrested window of the experimental tests. The simulation result of test 2-8 is shown in Figure 4.5(f). Here, the hydraulic fracture crossed the preexisting fracture, whereas in some parts, the preexisting fracture was dilated by the hydraulic fracture.

In summary, the results of the simulations were consistent with the experimental results, thus proveing the validity of the method in simulating hydraulic fracture phenomenon.

4.4 Summary

Chapter 4 describes the process by which experimental hydraulic fracture results were simulated to validate the numerical implementation of the viscoelastic constitutive model into PDLAMMPS. The model and the parameters were used and optimized based on experimental data and previous studies about the peridynamic simulation of concrete structures (Gheitanbaf, 2013; Tuniki, 2012). The hydraulic fracture simulation results were fit to the experimental results done by Zaho et al. (2008). This chapter has demonstrated the ability of the state-based peridynamic framework in simulating hydraulic fracture initiation and propagation in geological media. More importantly, this model will be useful in our simulation of hydraulic fracture phenomena using the PDLAMMPS open source software.

TABLE 4. 1 Rock mechanical parameters of the block

Symbol	Parameters	Value	Units
E	Young's modules	8.402	GPa
$\boldsymbol{v}$	Poisson's ratio	0.23	-
$\boldsymbol{\sigma_c}$	Unconfined compressive stress	28.34	MPa
K	Permeability	0.1	mD
∅	Porosity	1.85	%

TABLE 4. 2 The summary of the experimental tests and results of hydraulic fracture tests are presented, after (J. Zhou, Chen, Jin, & Zhang, 2008)

Type	Approaching Angle (deg)	$\boldsymbol{\sigma_v}$ (MPa)	$\boldsymbol{\sigma_H}$ (MPa)	$\boldsymbol{\sigma_h}$ (MPa)	Experimental Results	Simulation Results
2-1	90	20	10	5	Crossed	-
2-2	90	20	10	3	Crossed	-
2-4	60	20	10	3	Crossed	Crossed
2-6	60	20	13	3	Crossed	Crossed
S-1	60	20	15	0	Crossed	Crossed
2-8	60	20	8	5	Dilated	Crossed & Dilated
S-2	45	20	8	5	-	Dilated
2-3	30	20	10	5	Dilated	-
2-5	30	20	8	5	Dilated	-
2-7	30	20	13	3	Arrested	Arrested

TABLE 4. 3 Parameters of the viscoelastic simulation

Parameters	Value
G	5.3 GPa
S00	0.000126
$\boldsymbol{\alpha}$	0.1
$\boldsymbol{\delta}$	0.00075
Density	2300 kg/m^3
Lattice	0.00025 m
λ	0.0 1

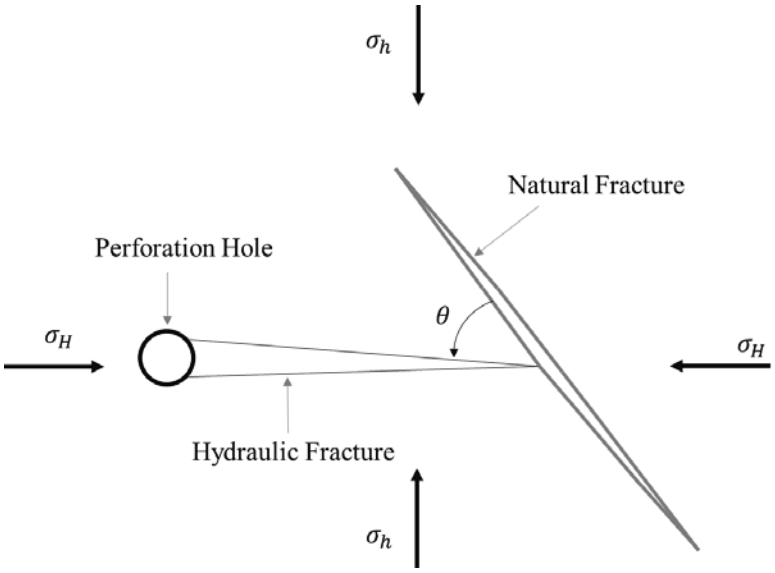

FIGURE 4. 1 Schematic of preexisting fracture affecting the propagation of hydraulic fracture, after (Zhou et al., 2008)

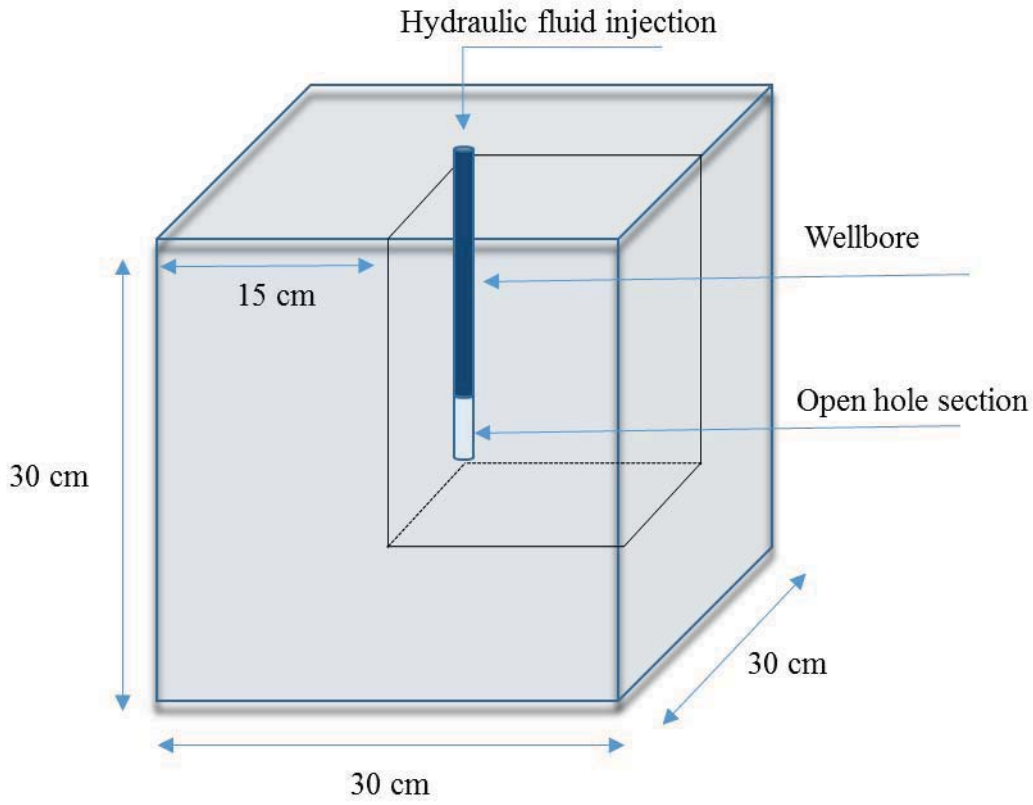

FIGURE 4. 2 Schematic of the test block and the length of open hole is 1 cm, after (Zhou et al., 2008))

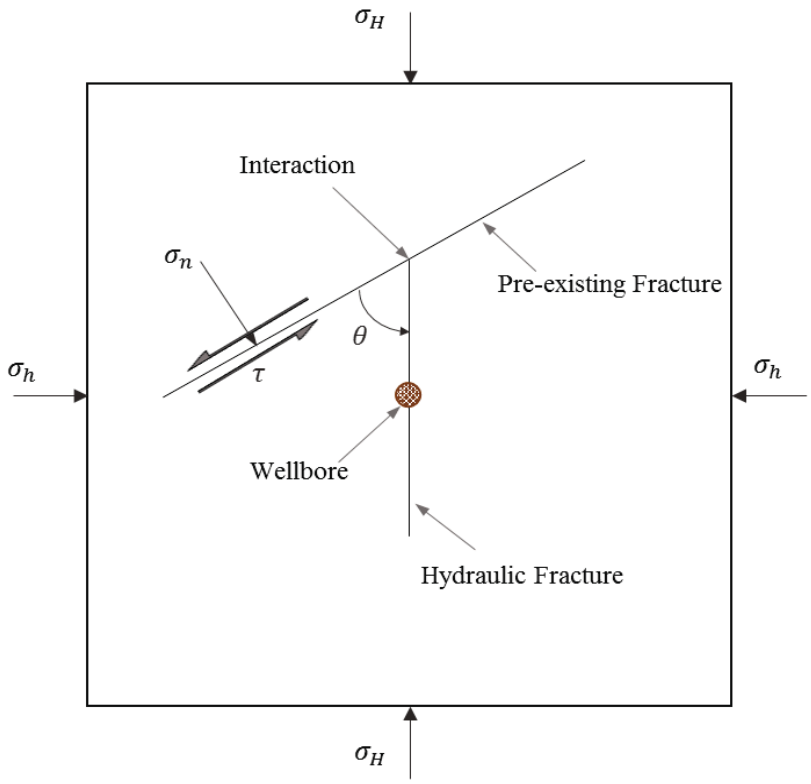

FIGURE 4. 3 Schematic of hydraulic fracture intersecting prefracture, after (Zhou et al., 2008)

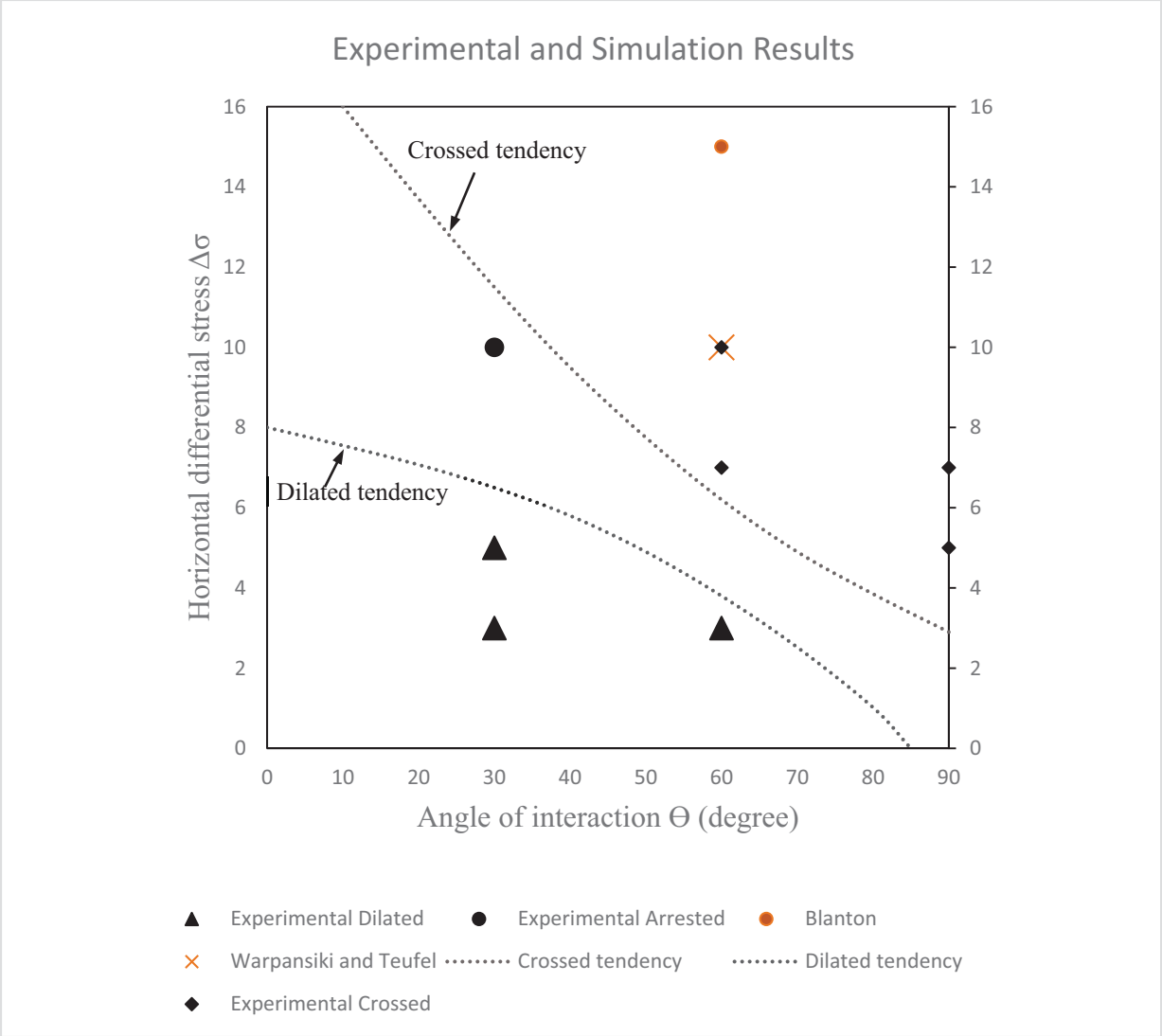

FIGURE 4. 4 Hydraulic fracture behavior of the Laboratory tests in a normal stress regime. Dilatation happened below the dilated tendency line, and crossing dominated above the crossed tendency line, after (Zhou et al., 2008)

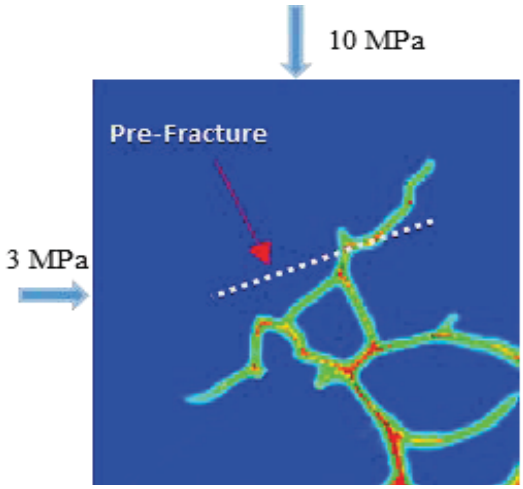

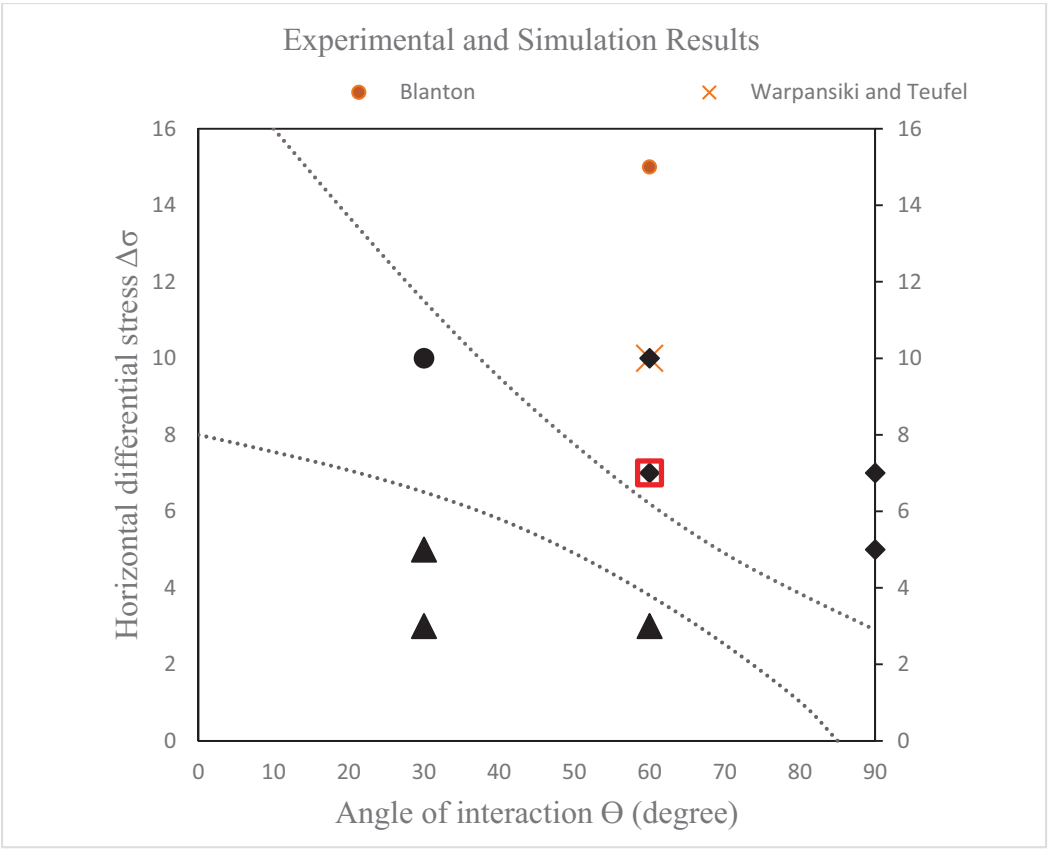

(a)

FIGURE 4. 5 Simulating the experimental tests. (a) Simulation result of experimental tests 2-4, (b) Simulation result of experimental tests 2-6, (c) Simulation result of a test with approach angle of 60° with horizontal stresses of 15 and 5 MPa, (d) Simulation result of a test with approach angle of 45° with horizontal stresses of 8 and 5 MPa, (e) Simulation result of experimental tests 2-7, (f) Simulation result of experimental tests 2-8.

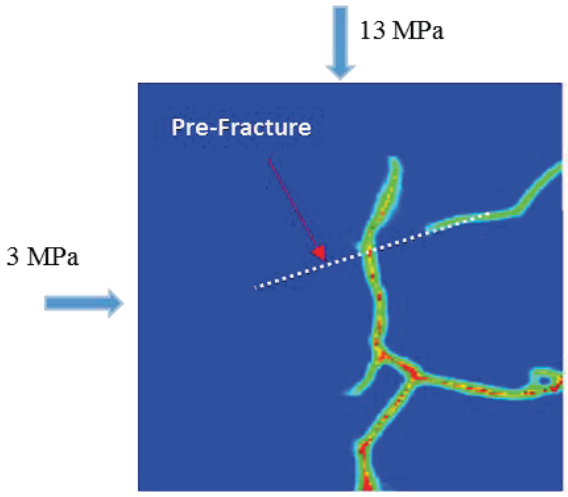

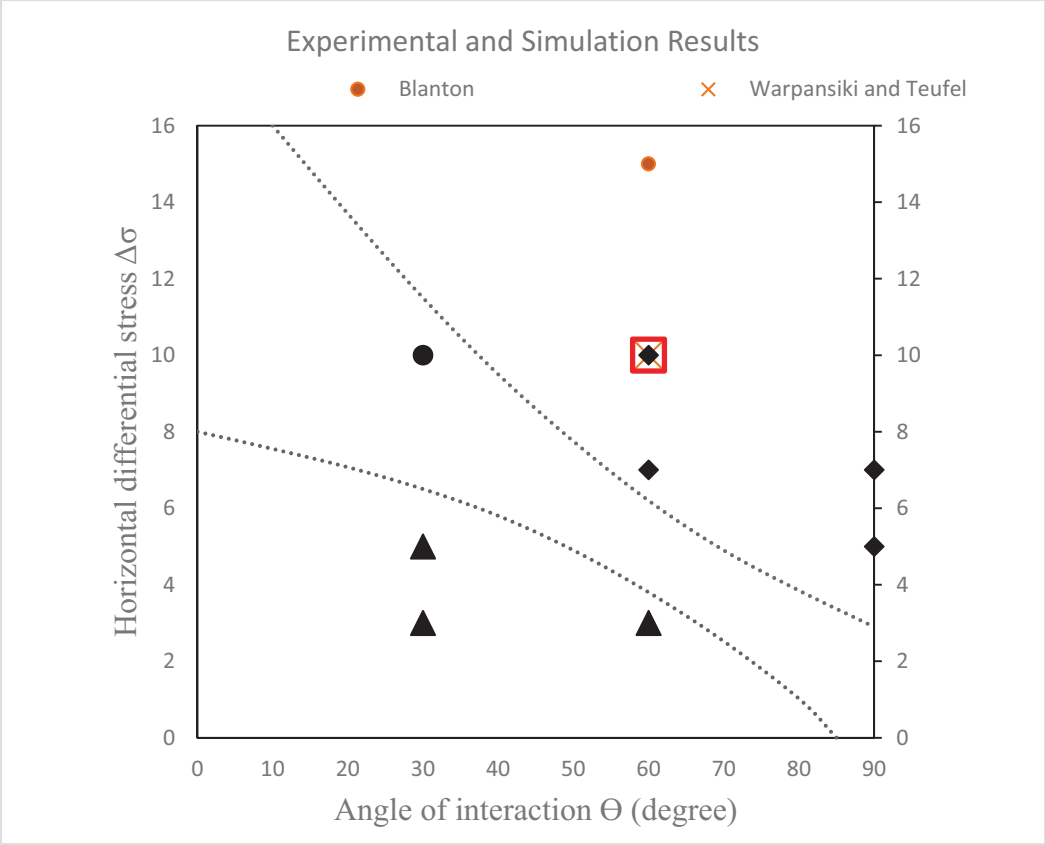

(b)

FIGURE 4. 5 Continued

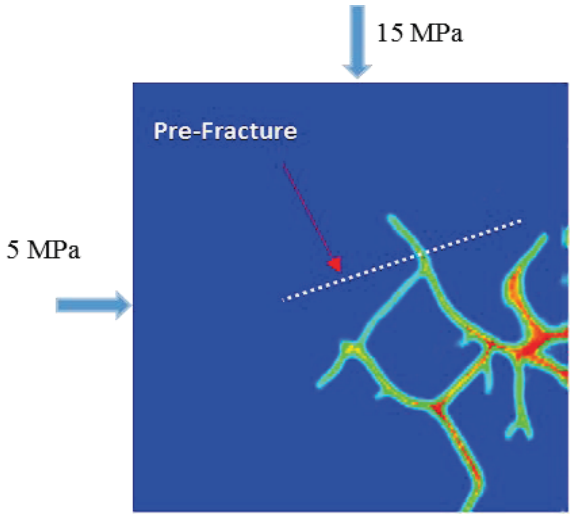

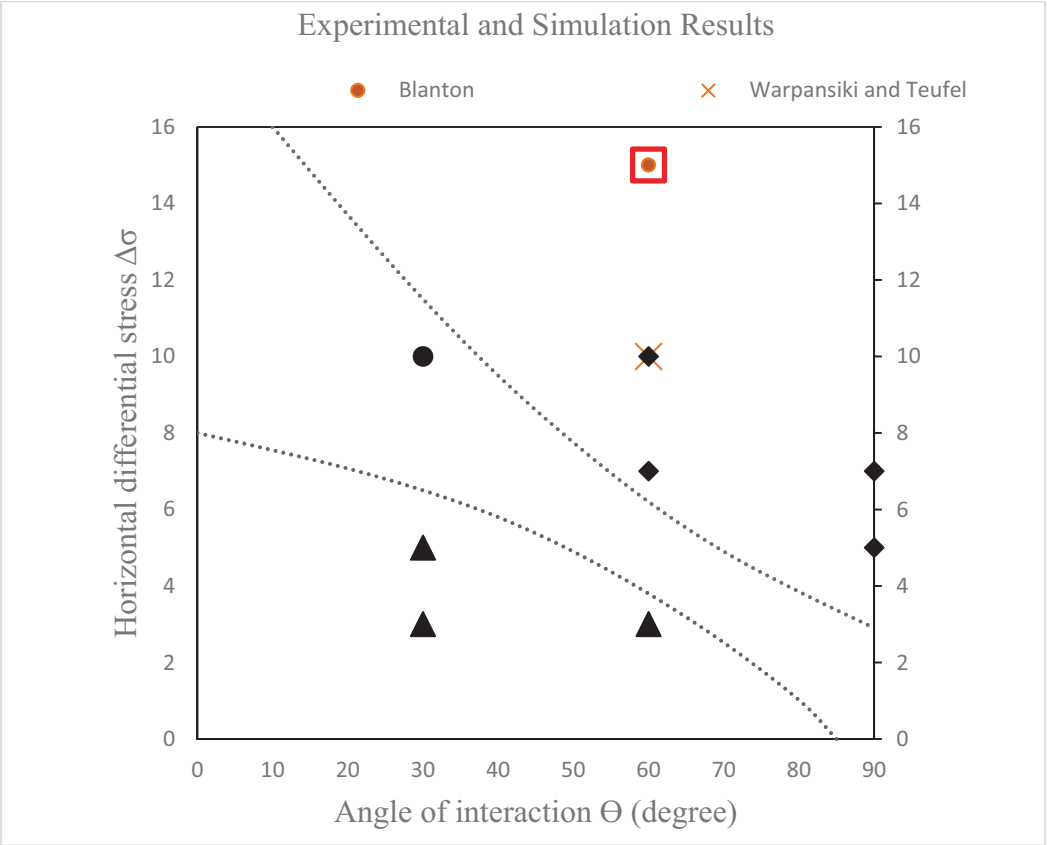

(c)

FIGURE 4. 5 Continued

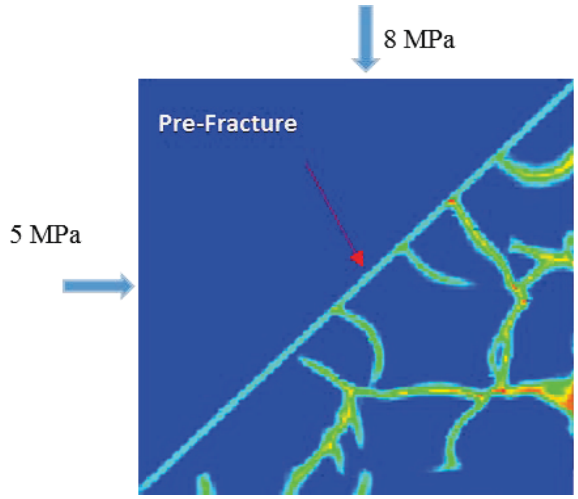

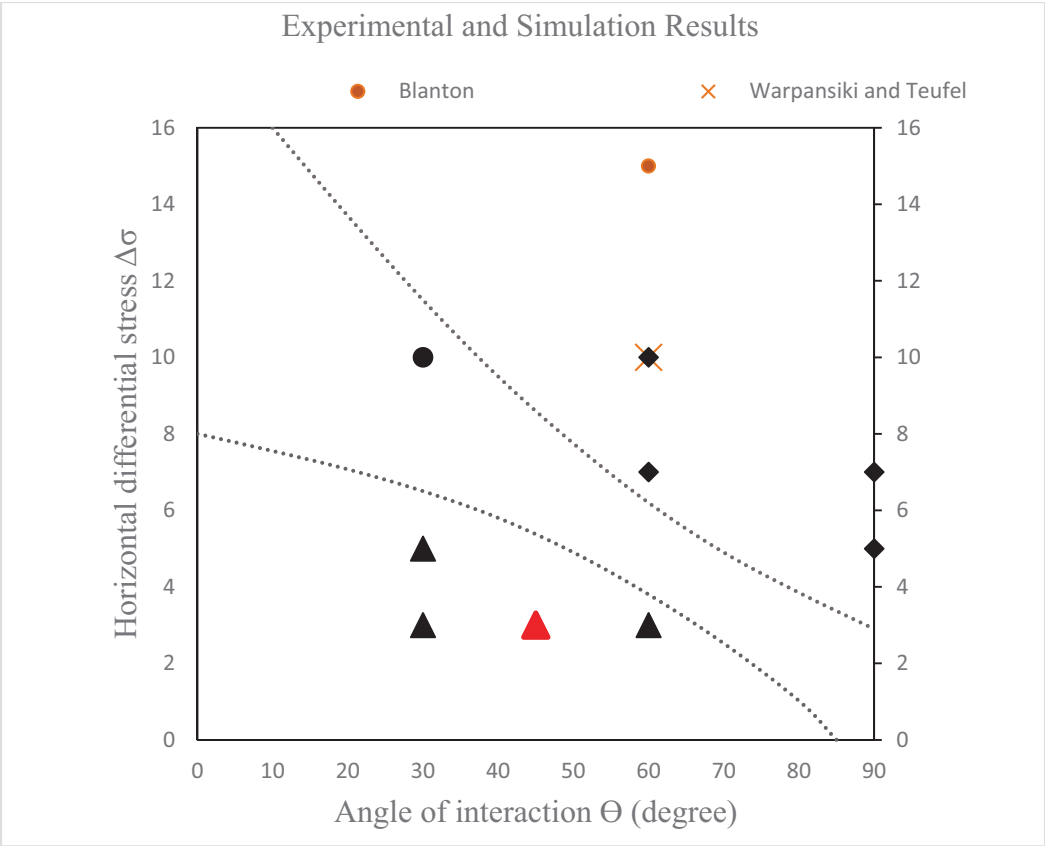

(d)

FIGURE 4. 5 Continued

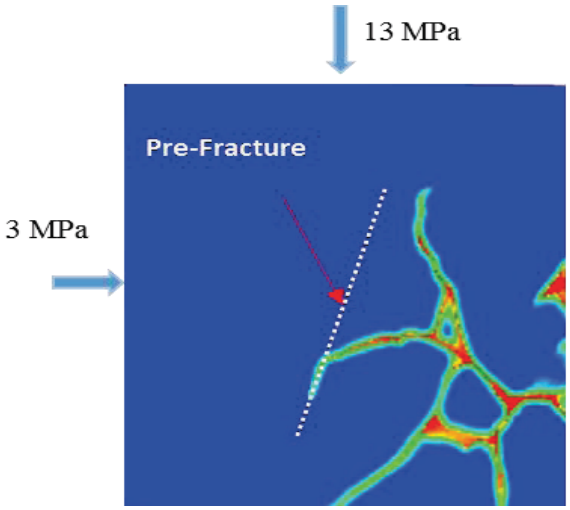

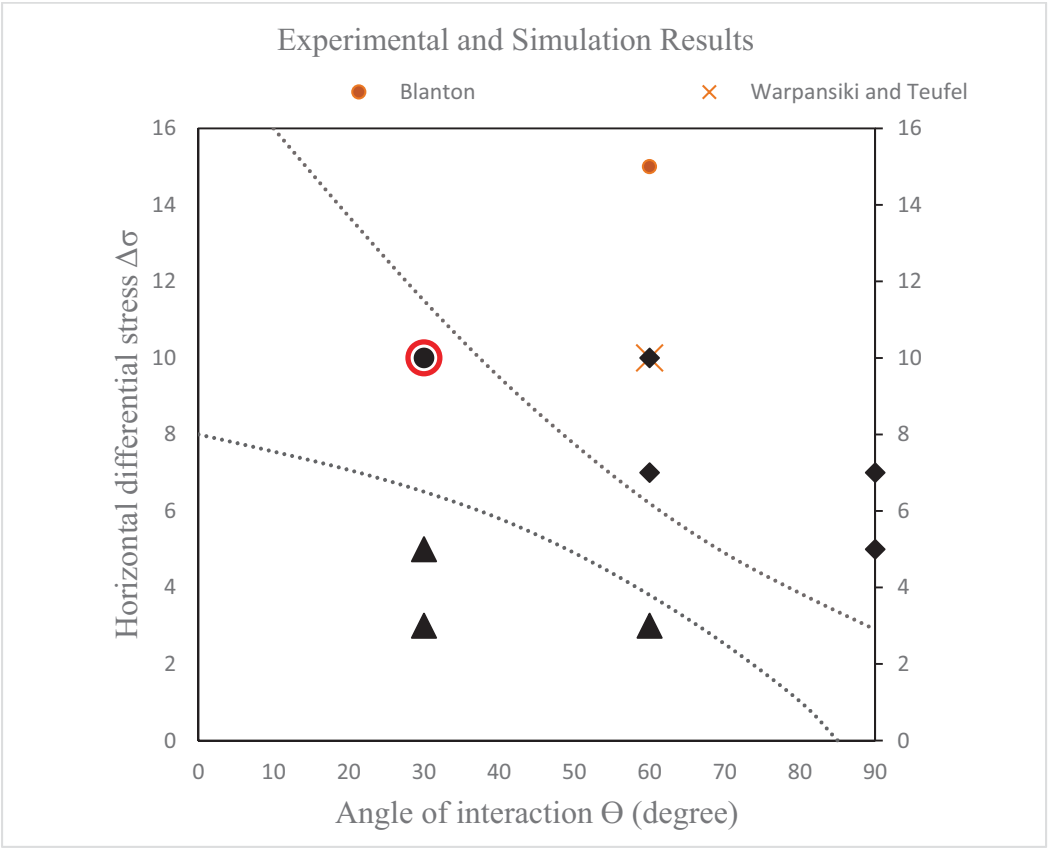

(e)

FIGURE 4. 5 Continued

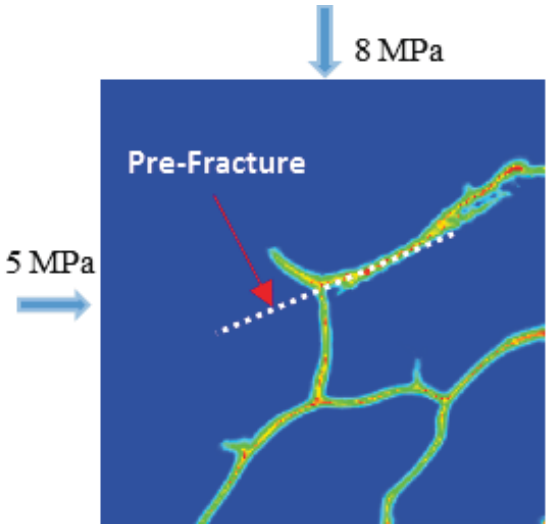

(f)

FIGURE 4. 5 Continued

CHAPTER 5

HYDRAULIC FRACTURE SIMULATION AND RESULTS

5.1 Numerical Implementation

In this study, PDLAMMPS open source software was used to simulate the hydraulic fracturing phenomena in a block of shale rock. For developing the code, the peridynamic model is discretized within LAMMPS (Plimpton, Thompson, & Crozier). A peridynamic model was performed on a three-dimensional domain (a 3D rectangular formation) with size of $0.08\,m \times 0.08\,m \times 0.08\,m$. A perforation hole with a diameter of 0.01 m was created in the geometry model. In this simulation, the block was assumed to be homogenous and isotropic. The geometry of the hydraulic fracturing phenomena is shown in Figure 5.1. The domain of the simulation was discretized with cubic lattices of particles with $1.25 \times 10^{-10} m^3$ volume. The method is meshfree where there are no geometrical connections between the particles (points or lattices). The mass density of a lattice cell is 2500 kg/m^3, and bulk modules are 10.6 GPa. The horizon, δ, is three times the lattice spacing.

Three different fluid injection rates, 0.33, 0.47, and 0.61 m^3/min, were applied to the perforation hole to compare the fracturing results achieved at different injection rates. The simulation was performed in constant volume and energy integration to update the position and velocity for atoms in the group per each time-step. The velocity and position

and the time-step was set to $5e10^{-7}$seconds. The total number of particles in this simulation was 4,173,281 with 498,324,794 total peridynamics bonds. The parameters of the simulation are shown in Table 5.1.

In this study, the linear viscolesaticity model implemented in PDLAMMPS was used to investigate the process described above. The total extension state in the formation was composed of two parts: volumetric and deviatoric extensions. In the peridynamic theory, damage is revealed by bond breakage; when the stretch in a bond exceeds the critical limit, s_0, the bond will break. Once a bond breaks, it cannot be recovered and it will no longer tolerate force. To investigate the damage and effects of hydraulic fracturing on the formation, two sets of data, damage per atom and dilatation per atom, were computed and extracted. The results of the simulation are shown in the Section 5.2.

5.2 Computational Results

This section presents the numerical results of the hydraulic fracturing simulation described in Section 5.1. The simulation results were investigated by comparing the damage values in three directions ($\theta = 0°, 45°, 90°$) within a certain distance from the center of the perforation hole ($\frac{r}{r_0} = 1, 2, 3, 4$). Figure 5.1 shows the location of the tracking particles in three planes perpendicular to the perforation hole. As expected, the plane closest to the perforation hole exhibited the most damage, while further away from the perforation hole, the damage around the whole decreases.

Figure 5.2 shows the propagation of fractures during different time-steps and injection rates. Zones (bonds) with higher damage magnitudes are colored with warmer (red) colors while blue colors indicate nondamage zones. It is clear that by increasing the

time-step of the simulation, the area of the fractured zone around the hole increases and propagates longer. As shown in Figure 5.2, the bonds break symmetrically because of material homogeneity. At the beginning of the simulation, fractures started just next to the perforation hole and propagated outside, near to the boundary of the model. During the simulation time-steps, the formation just next to the hole was crushed, but on the outside of the model, the cracks propagated separately.

In the three different simulations, displacement and fracture conditions enforced by three injection rates were different in shape and value. The symmetry-breaking pattern around the perforation hole resulted from the homogenous and isotropic geological media used in the simulations. It was concluded that the symmetric fracturing does not depend on the regularity of the lattice size if the horizon, δ, is large enough. Further, the method is not restricted to fixed structured grids. Hence, for creating different lattice size in the simulation, an initial lattice size with randomly perturbed distance can be used.

Figure 5.3 shows the damage zones in three planes at the same time-step (1200 simulation time-steps) for the simulations with injection rates of 0.33, 0.47, and 0.61 m^3/min. By getting farther from the bottom hole in y direction to the end of the model, the damage area decreased, whereas the damage area close to the bottom hole was significantly larger. The fracture growth results presented in Figure 5.3 (plane 3) show the bond breakages in sections perpendicular to the fracture propagations. The higher injection rate caused higher density of damaged atoms in the section.

Initiation and propagation of fractures in the peridynamic model are more explicit than in other modeling methods. The peridynamic method does not need any additional formulation or remeshing to simulate a growing fracture. In other words, once a fracture

forms, the model does not need any modification to process the fracturing phenomenon, and the behavior of the model can be obtained on any broken bond or particle. Fractures are formed as groupings of bond breakages. In Figures 5.4-5.6, the results of the damage and dilatation are presented in different particles. As shown in Figure 5.4, the high injection rate causes greater damage in the formation. In addition, damage initiated much sooner at higher injection rates (green curves, 0.61 m^3/min). On the other hand, the blue curves illustrate that the simulations with the lowest injection rate (0.33 m^3/min) caused less damage. Indeed, in the farthest planes, complete damage did not occur (damage < 1).

Microscopic studies conducted on hydraulic fracturing phenomena have shown that shear dilatation is one of most important factors that causes fracture initiation and propagation and permeability enhancement in hydraulic fracturing phenomena. The shear stress occurs because of fluid injection that causes the offset of two fracture surfaces, allowing fluid flow between them. In addition, the sliding of fracture surfaces on each other causes to dilate of the aperture normal to the surfaces. The physical process of the shear slippage and dilatation is shown in Figure 5.7 (Hossain, Rahman, & Rahman, 2002). Therefore, dilations within a complex fracture network cause shear movements on other fractures close to the dilated fracture. This results in a combination of shear and tensile dilation. Figures 5.8-5.10 show the dilatation in the middle plane during the different time-steps of simulation with different injection rates. As shown in Figures 5.8-5.10, the simulation with an injection rate of 0.61 m^3/min caused the maximum dilatation in the model (green curves), especially during the last steps of the simulation. In addition, dilatation in that simulation initiated sooner than two other injection rates. In other words, the volumetric and deviatoric extensions in 0.61 m^3/min injection are bigger, and initiate much sooner than in the 0.33, m^3/min injection rate. Therefore, it causes higher damage

area at the highest injection rate.

The most important advantage of the peridynamic approach over other methods in fracture modeling is that it does not require any additional formulation that determine when a crack should grow, its velocity, direction, and branching, and relationship between length and width of the crack. The equation of motion and the response function deal with all of these phenomena, which incorporate damage at the bond level. Notably, the method does not need to compute a stress intensity factor at a crack tip in order to investigate the fracturing propagation. By using the same response function either on or off of a crack surface, no other constitutive equation is required to deal with opposite sides of a crack separately. Therefore, only one response function is used to treat any number of cracks, including the material interactions.

Figure 5.11 (a, b, and c) shows the histogram of the damaged atoms number in each injection rate based on different damage intervals. In this figure, the interval (0.9–1) shows the complete damage in the simulation, where the interval (0–0.1) refers to the area without any damage. Shown in Figure 5.11(d), the injection rate 0.61 m^3/min caused the highest complete damage (0.9–1) with 5.24% of the total number of atoms. The other two injection rates, 0.47 and 0.33 m^3/min, caused less damage in that range with 2.30% and 0.36% of total number of atoms, respectively. On the other hand, the injection rate 0.33 m^3/min has the maximum value undamaged zone (0–0.1) with 41.72% of the total number of atoms, and two other injection rates, 0.47 and 0.61 m^3/min, have undamaged zones of 23.42% and 11.31% of the total number of atoms, respectively (see Table 5.2 and Figure 5.11(d)).

TABLE 5. 1 Parameters of the viscoelastic simulation

Parameters	Value
K	10.6 GPa
G	1 GPa
S00	0.0005
α	0.1
δ	0.0015
Density	2500 kg/m^3
Lattice	0.0005
Lattice Vol.	1.25e-10 m^3

TABLE 5. 2 Number of atoms and their percentage in each damage interval at the end of simulation

Interval	Number of atoms in each interval			Percentage of atoms in each interval		
	0.33 (m^3/min)	0.47 (m^3/min)	0.61 (m^3/min)	0.33 (m^3/min)	0.47 (m^3/min)	0.61 (m^3/min)
0-0.10	1741298.00	977527.00	472148.00	41.73	23.42	11.31
0.10-0.20	207330.00	188197.00	147282.00	4.97	4.51	3.53
0.20-0.3	171196.00	172792.00	144576.00	4.10	4.14	3.46
0.3-0.4	136435.00	143360.00	145911.00	3.27	3.44	3.50
0.4-0.5	167635.00	165994.00	152689.00	4.02	3.98	3.66
0.5-0.6	283954.00	202415.00	197458.00	6.80	4.85	4.73
0.6-0.7	409953.00	517574.00	296376.00	9.82	12.40	7.10
0.7-0.8	555528.00	688707.00	880805.00	13.31	16.50	21.11
0.8-0.9	484602.00	1020582.00	1517255.00	11.65	25.03	38.37
0.9-1	15332.00	96115.00	218763.00	0.37	2.30	5.24

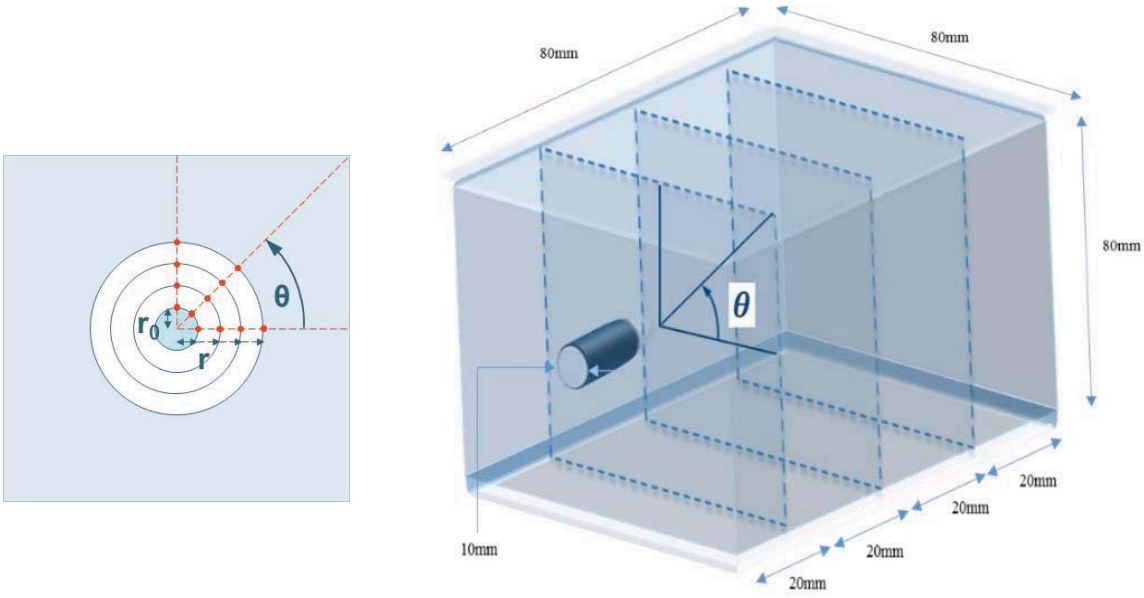

FIGURE 5. 1 Geometry of simulation, planes, and location of the investigation points (Nadimi & Miskovic, 2015)

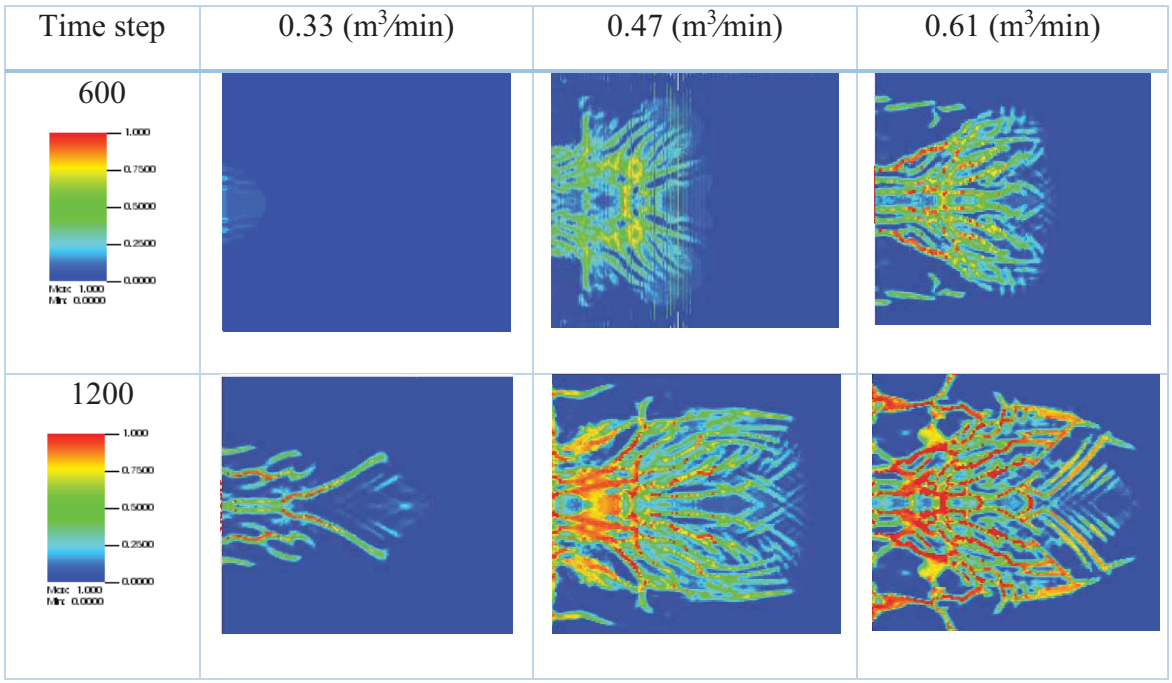

FIGURE 5. 2 Side view of the fracture propagation in two different time-steps for three different injection rates (0.33, 0.47, and 0.61 m^3/min)

Time step	0.33 (m^3/min)	0.47 (m^3/min)	0.61 (m^3/min)
1200 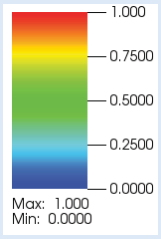	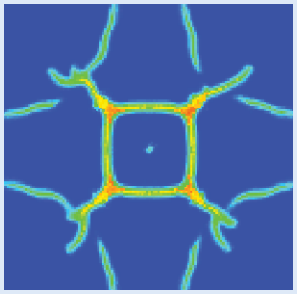	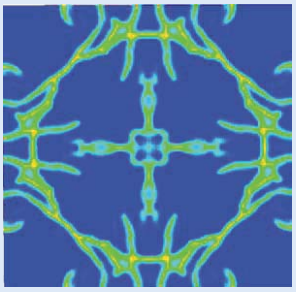	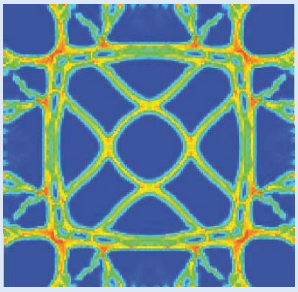

FIGURE 5. 3 Cross sections of the fracture propagation in the second plane for three different injection rates 0.33, 0.47, and 0.61 (m^3/min) in the same time-step (1200)

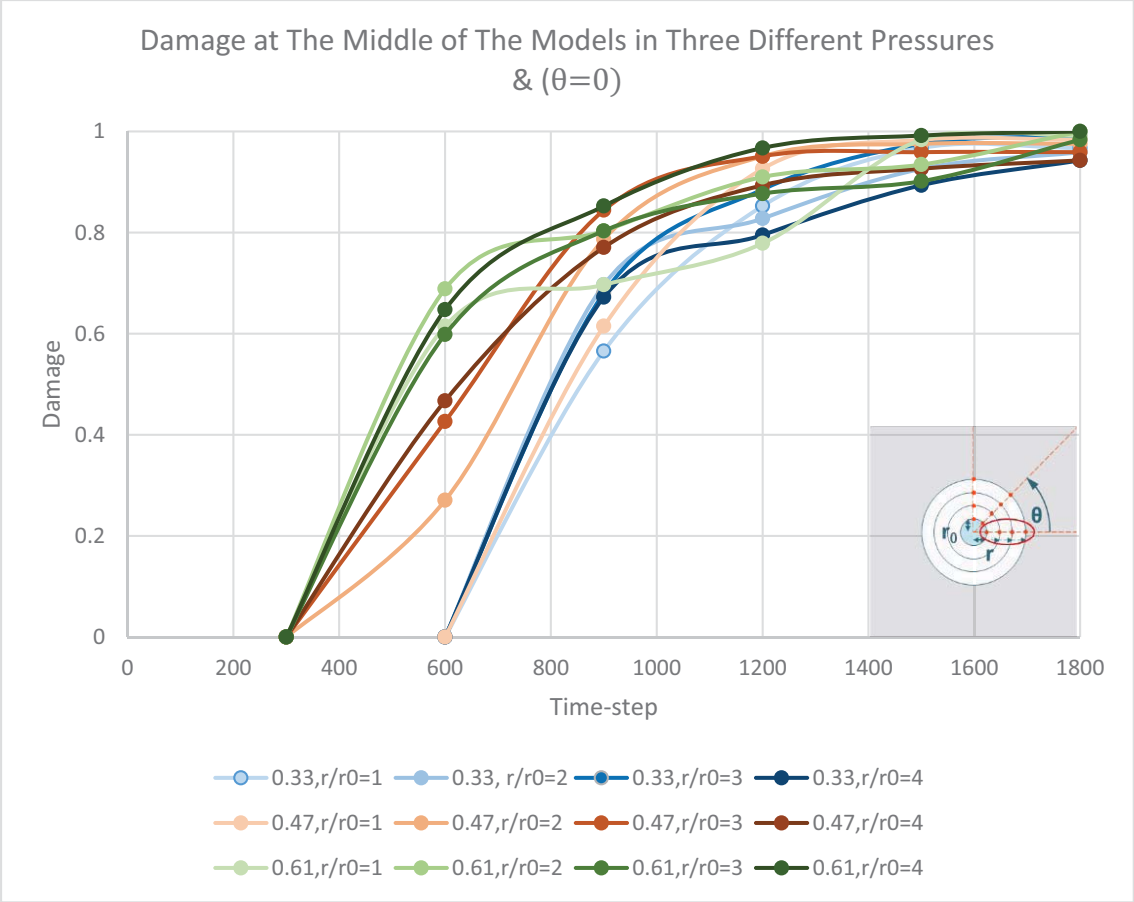

FIGURE 5. 4 Damage-time-step plot at 0° direction

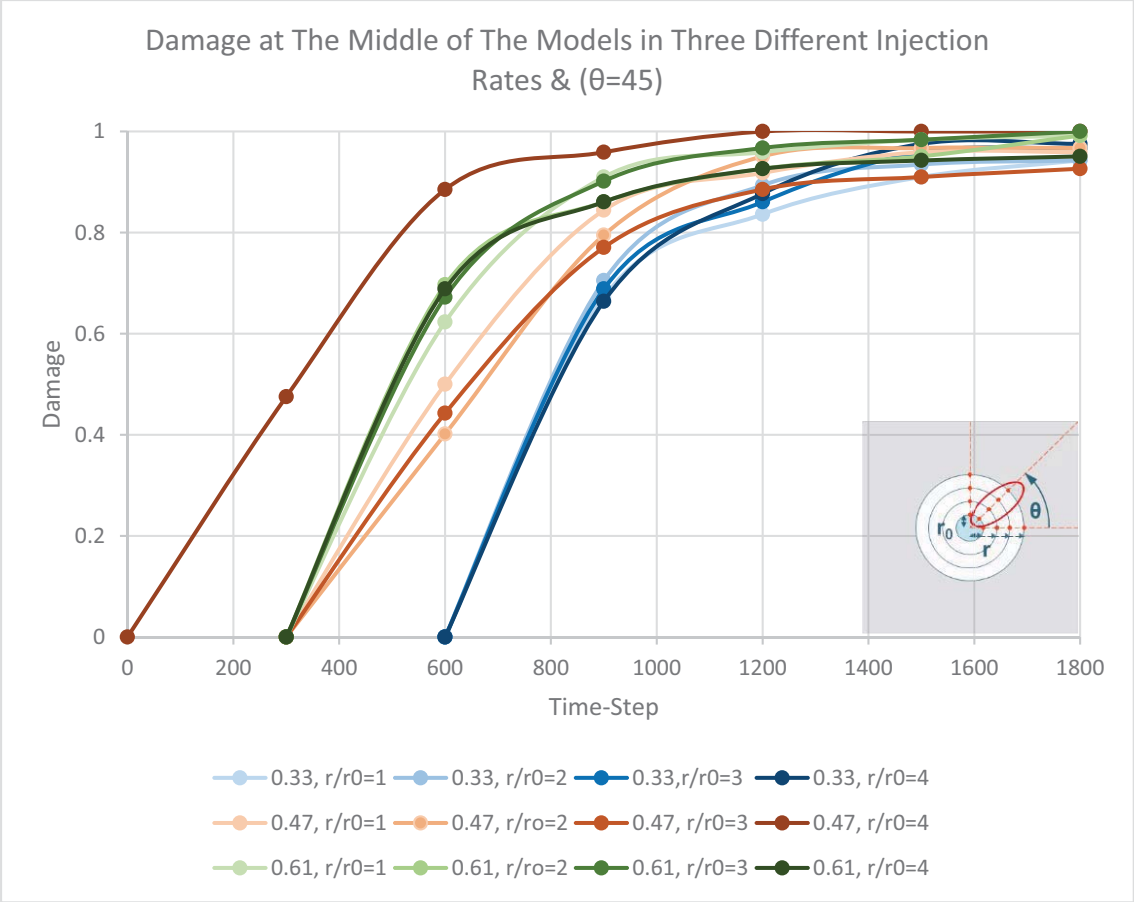

FIGURE 5. 5 Damage-time-step plot at 45° direction

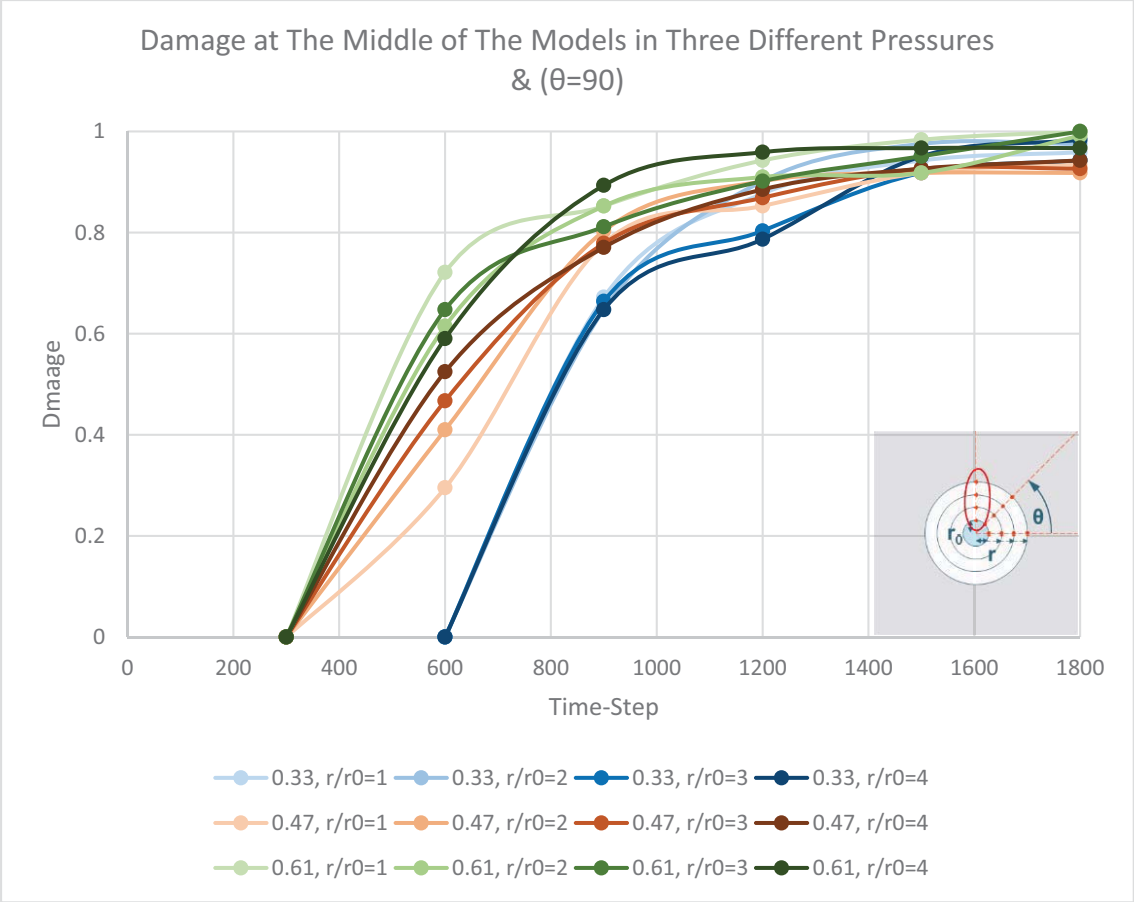

FIGURE 5. 6 Damage-time-step plot at 90° direction

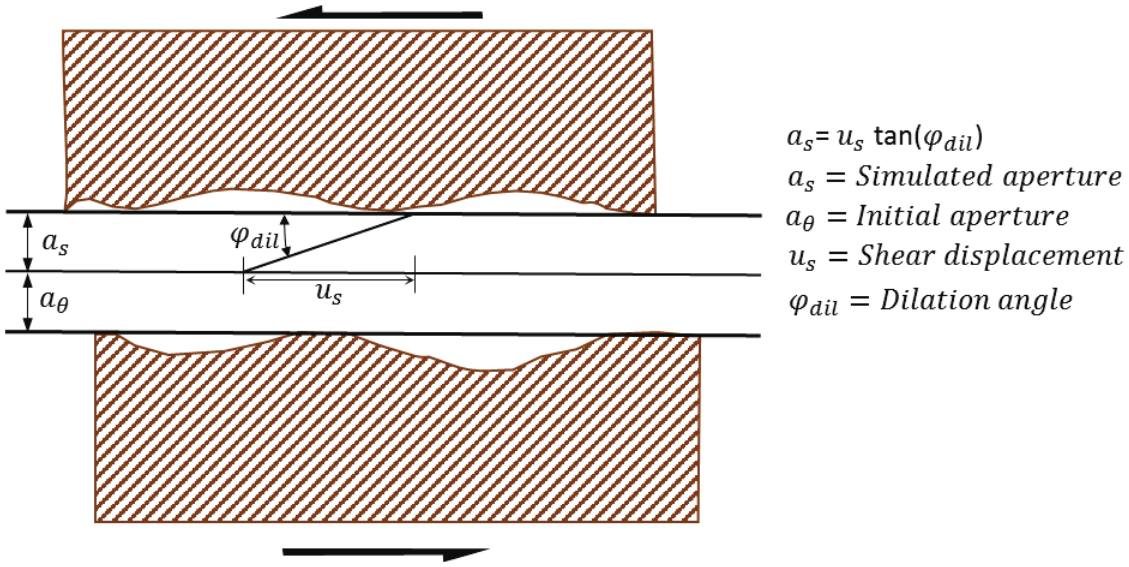

FIGURE 5. 7 The physical process of the shear slippage and dilation, after (Hossain et al., 2002)

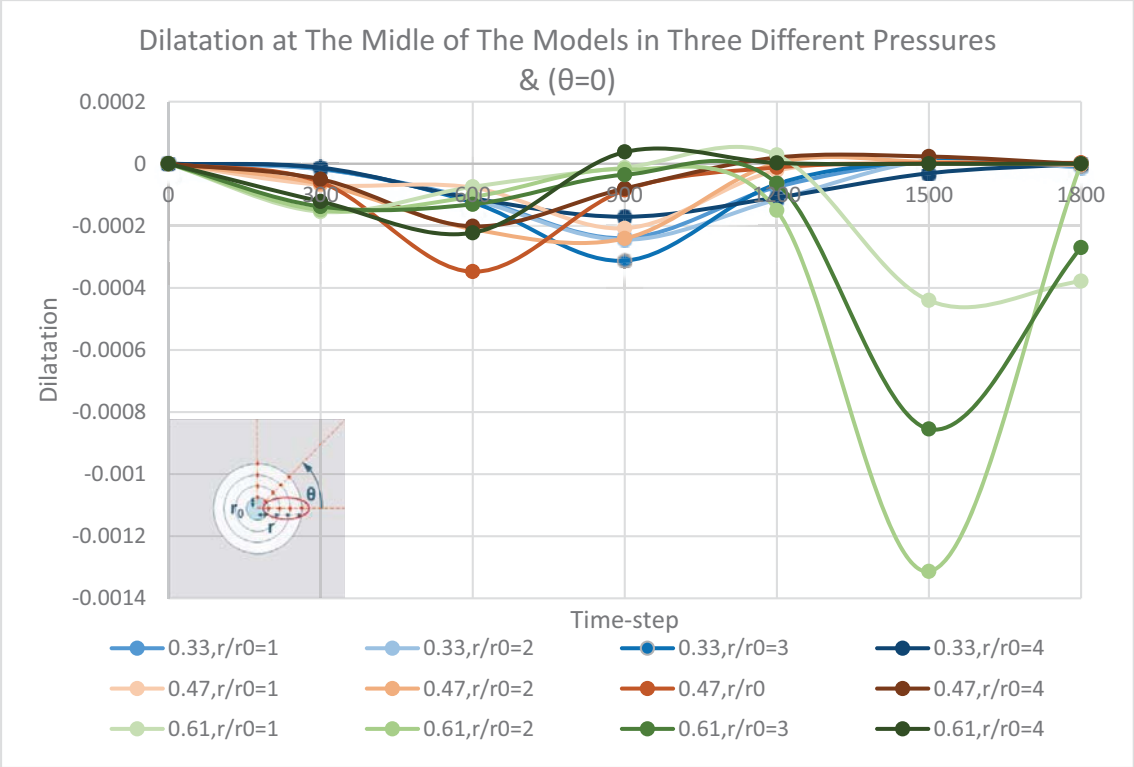

FIGURE 5. 8 Dilatation-time-step plot at 0° direction- Dilatation-time-step plot in the middle plane with three different simulations with inject rates of (0.33, 0.47, and 0.61 m^3/min)

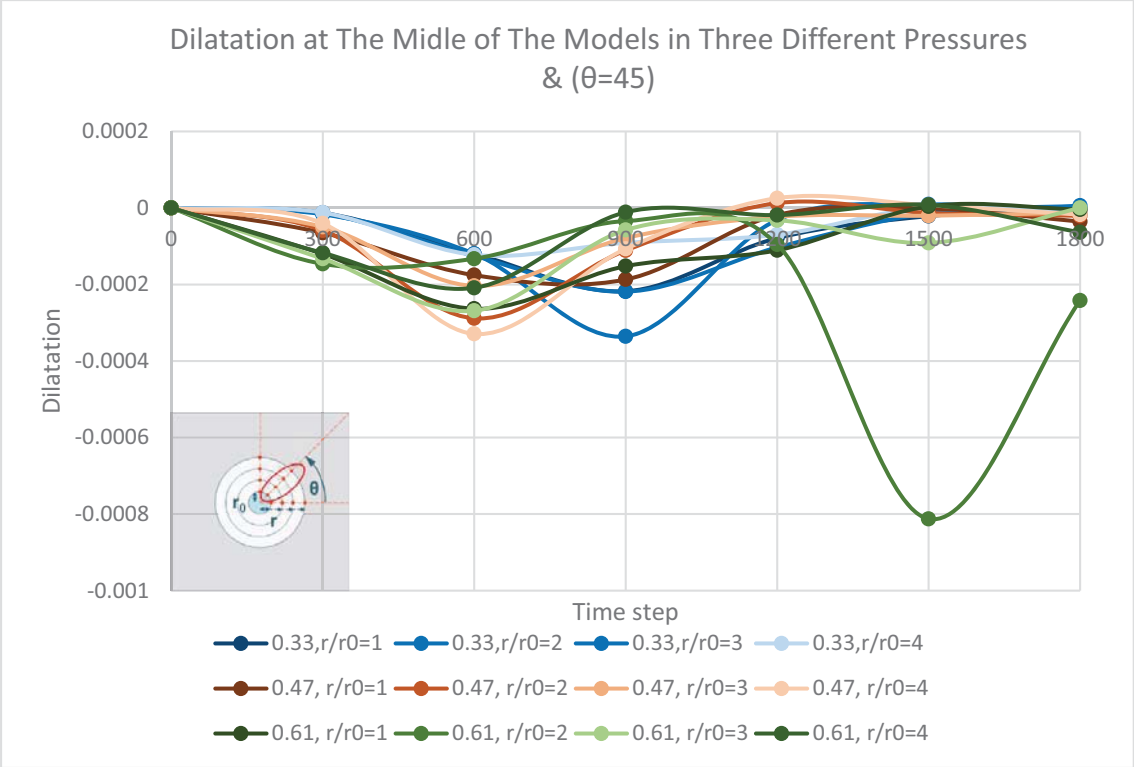

FIGURE 5. 9 Dilatation-time-step plot at 45° direction- Dilatation-time-step plot in the middle plane with three different simulations with inject rates of (0.33, 0.47, and 0.61 m^3/min)

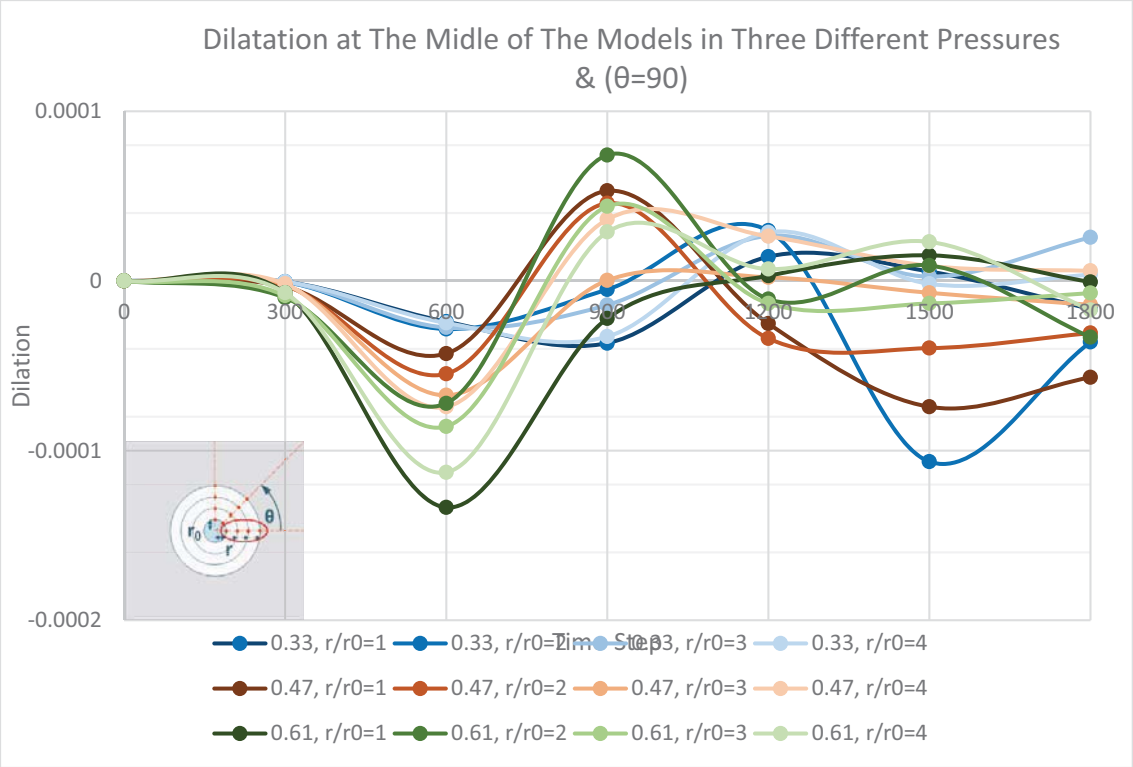

FIGURE 5. 7 Dilatation-time-step plot at 90° direction. Dilatation-time-step plot in the middle plane with three different simulations with inject rates of (0.33, 0.47, and 0.61 m^3/min)

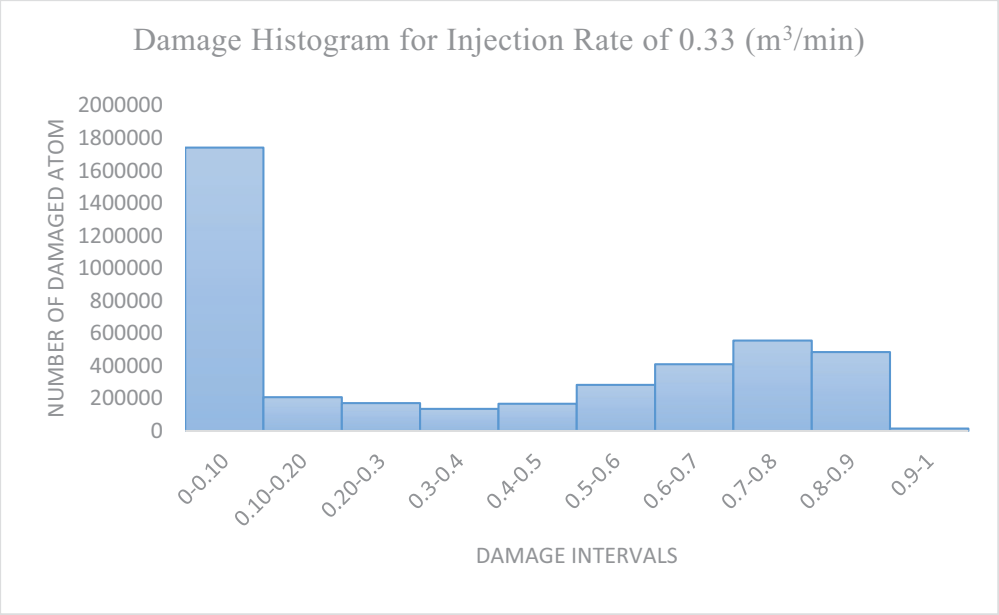

(a)

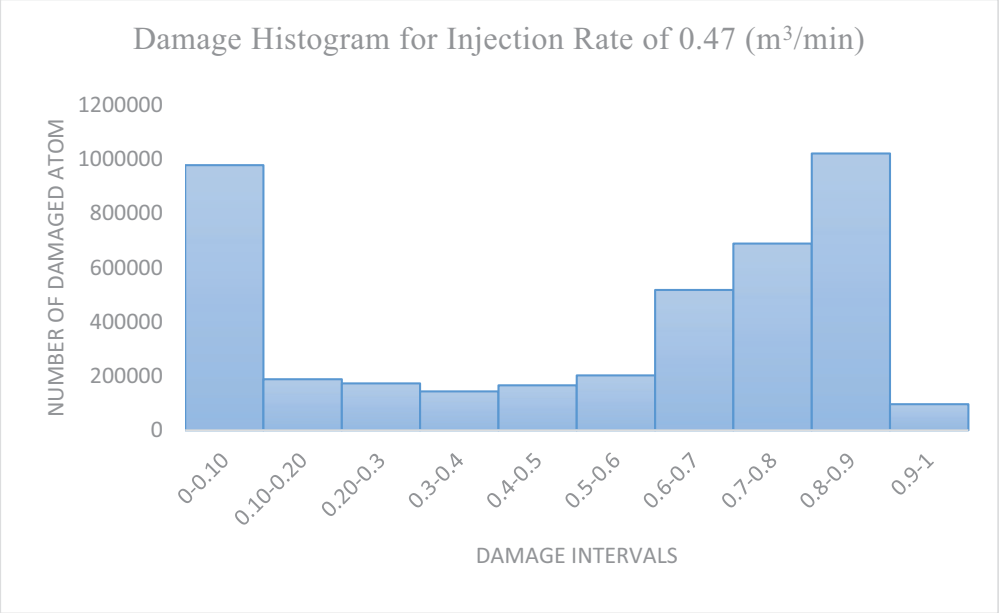

(b)

FIGURE 5. 8 Histogram of damage in each injection rate at 1800 time-step, (a) 0.33 m^3⁄min, (b) 0.47 m^3⁄min, (c) 0.61 m^3⁄min, and (d) total

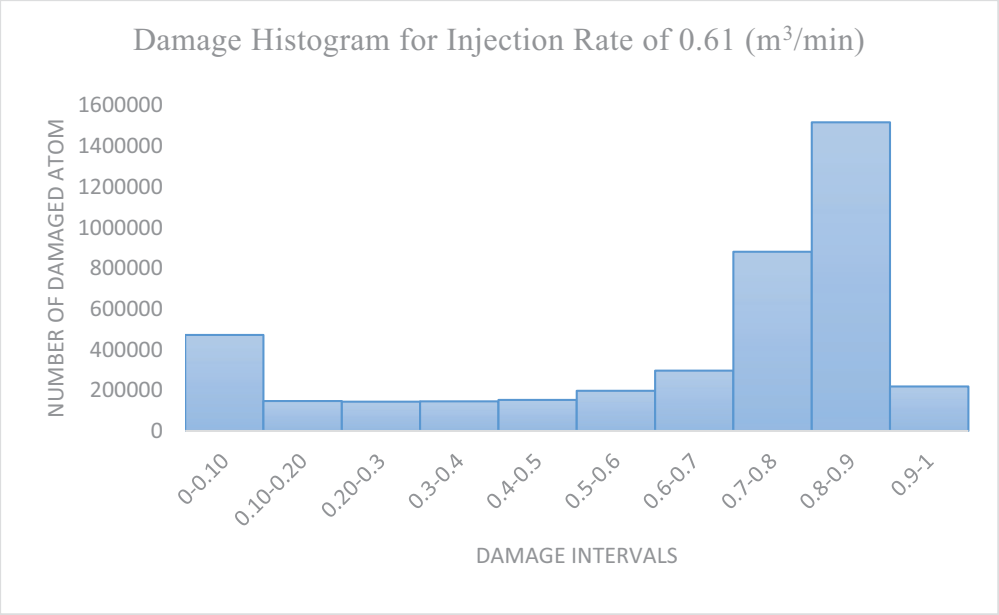

(c)

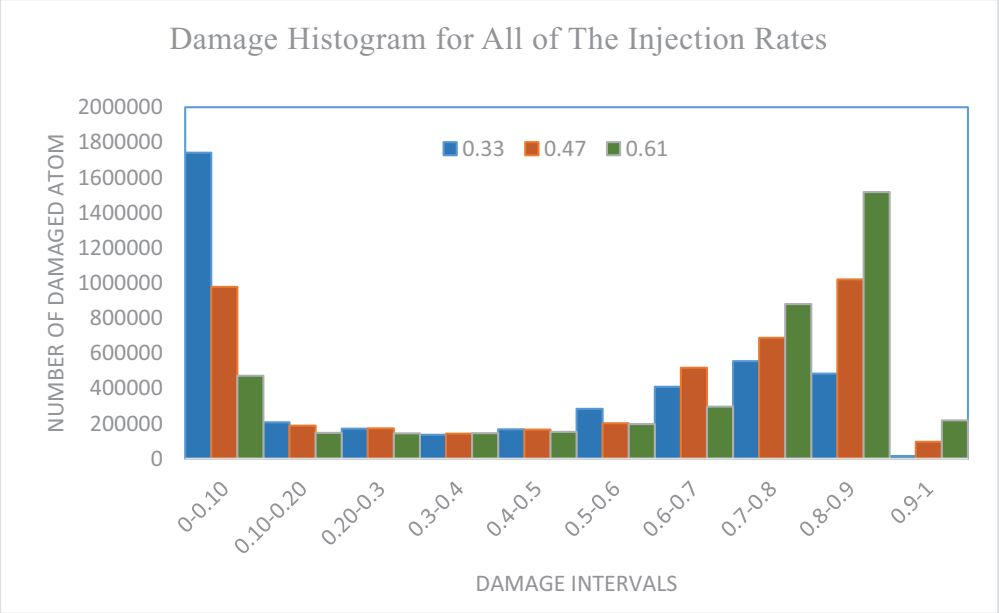

(d)

FIGURE 5. 8 Continued

CHAPTER 6

CONCLUSION

The primary aim of this research was to evaluate the utility of peridynamic theory for simulating hydraulic fracture phenomenon. The state-based peridynamic model was developed and hydraulic fracture simulation was performed under three different injection rates. For validating and calibrating the model, results from an experimental study performed by Zhou et al. (2008) were used.

The peridynamic theory is a modification of the equation of motion in solid mechanics, which is mainly used for modeling discontinuous media, such as fractured rock. In this theory, instead of the partial differential equations that are used in classical formulations, integral equations are utilized, helping to define discontinuities without any reformulation of the model. There are several aspects of the peridynamic theory that make it suitable for modeling a coupled complex thermal-hydraulic-mechanical process without using additional failure criteria or crack-growth laws because the peridynamic motion equation deals with all of the interactions in a material, including discontinuities. One of the most important advantages of the peridynamic method over other numerical methods is that the same equation of motion is used to model the behavior of a heterogeneous medium, regardless of any damage sites or discontinuities.

As confirmed in this study, the peridynamic method is capable of predicting the

hydraulic fracture process, including fracture initiations and propagation, and geometry of the hydraulic fractures. This method also has the benefit of being a meshfree method, which significantly reduces the computational cost of the simulation. Hence, peridynamics shows great promise for simulating highly complex damage processes in heterogeneous and/or discontinuous porous media.

This study used a set of data from experimental research performed by Zhou et al. (2008) to validate the model. The similarities between the simulation results and the experimental results were presented in this thesis, along with investigation of the influences of differential horizontal stress and the approach angle of a preexisting fracture on the hydraulic fracture. In the lower approach angles and differential horizontal stress, the preexisting fracture was dilated by the hydraulic fracture; in higher approach angles with higher differential horizontal stress, the hydraulic fracture crossed the preexisting fracture. In some cases, such as a simulation with a 45° approach angle and differential horizontal stress of 3 MPa, the hydraulic fracture was arrested by the preexisting fracture. Comparing the simulation and experimental results shows that there is a good match between the two.

The simulation results for three different injection rates were also reported in this study. It was found that the average permeability of a stimulated reservoir increases with the higher injection rate and as a result of the fractured area growth. The hydraulic fracturing phenomenon causes dilatation within the fracture network, causing fracture propagation to increase significantly. The damage in the simulation was computed based on damage per atom and dilation per atom. Shear dilatation is one of most the important factors that causes fracture propagation and increases the fracture aperture. In this study, the injection rate of 0.61 m^3/min led to maximum dilatation, and maximum damage area as well. In addition, it caused the highest complete damage (0.9–1) with 5.24% of the total

number of atoms.

Modeling the hydraulic fracturing process using peridynamics can provide unique insight into the initiation and propagation of cracks in geological materials. This study avoids the typical assumptions of Darcy flow and effective stresses. In future work, we will try to introduce these kinds of assumptions to the model and modify the porous media based on the actual data and hydraulic facture job condition.

The simulation of hydraulic fracturing in a discontinuous medium shows that the peridynamic approach is capable of modeling a naturally fractured geological formation as well as the interaction between hydraulic fracture and preexisting fracture. In addition, the peridynamic simulations of hydraulic fracturing phenomena present promising results in predicting fracture initiation and propagation.

REFERENCES

Adachi, J., Siebrits, E., Peirce, A., & Desroches, J. (2007). Computer simulation of hydraulic fractures. *International Journal of Rock Mechanics and Mining Sciences, 44*(5), 739-757.

Agwai, A., Guven, I., & Madenci, E. (2012). *Failure prediction in fully coupled thermal and deformational fields with peridynamics.* Paper presented at the Electronic Components and Technology Conference (ECTC), 2012 IEEE 62nd.

Alali, B., & Lipton, R. (2012). Multiscale dynamics of heterogeneous media in the peridynamic formulation. *Journal of Elasticity, 106*(1), 71-103.

Allaire, G. (1992). Homogenization and two-scale convergence. *SIAM Journal on Mathematical Analysis, 23*(6), 1482-1518.

Askari, E., Bobaru, F., Lehoucq, R., Parks, M., Silling, S., & Weckner, O. (2008). *Peridynamics for multiscale materials modeling.* Paper presented at the Journal of Physics: Conference Series.

Baca, R., Arnett, R., & Langford, D. (1984). Modelling fluid flow in fractured-porous rock masses by finite-element techniques. *International Journal for Numerical Methods in Fluids, 4*(4), 337-348.

Bai, M., Green, S., & Suarez-Rivera, R. (2005). *Effect of leakoff variation on fracturing efficiency for tight shale gas reservoirs.* Paper presented at the Alaska Rocks 2005 The 40th US Symposium on Rock Mechanics (USRMS).

Barenblatt, G. I. (1962). The mathematical theory of equilibrium cracks in brittle fracture. *Advances in Applied Mechanics, 7*(1), 55-129.

Belytschko, T., Chen, H., Xu, J., & Zi, G. (2003). Dynamic crack propagation based on loss of hyperbolicity and a new discontinuous enrichment. *International Journal for Numerical Methods in Engineering, 58*(12), 1873-1905.

Biot, M. A. (1941). General theory of three-dimensional consolidation. *Journal of Applied Physics, 12*(2), 155-164.

Biot, M. A. (1955). Theory of elasticity and consolidation for a porous anisotropic solid. *Journal of Applied Physics, 26*(2), 182-185.

Bishop, J. E., Martinez, M. J., & Newell, P. (2012). *A finite-element method for modeling fluid-pressure induced discrete-fracture propagation using random meshes.* Paper presented at the 46th US Rock Mechanics/Geomechanics Symposium.

Blanton, T. (1986). *Propagation of hydraulically and dynamically induced fractures in naturally fractured reservoirs.* Paper presented at the SPE Unconventional Gas Technology Symposium.

Bobaru, F., & Duangpanya, M. (2010). The peridynamic formulation for transient heat conduction. *International Journal of Heat and Mass Transfer, 53*(19), 4047-4059.

Bobaru, F., & Duangpanya, M. (2012). A peridynamic formulation for transient heat conduction in bodies with evolving discontinuities. *Journal of Computational Physics, 231*(7), 2764-2785.

Boutt, D. F., Cook, B. K., McPherson, B. J., & Williams, J. (2007). Direct simulation of fluid-solid mechanics in porous media using the discrete element and lattice-Boltzmann methods. *Journal of Geophysical Research: Solid Earth (1978–2012), 112*(B10).

Bower, K., & Zyvoloski, G. (1997). A numerical model for thermo-hydro-mechanical coupling in fractured rock. *International Journal of Rock Mechanics and Mining Sciences, 34*(8), 1201-1211.

Breitenfeld, M., Geubelle, P., Weckner, O., & Silling, S. (2014). Non-ordinary state-based peridynamic analysis of stationary crack problems. *Computer Methods in Applied Mechanics and Engineering, 272,* 233–250.

Camacho, G., & Ortiz, M. (1996). Computational modelling of impact damage in brittle materials. *International Journal of Solids and Structures, 33*(20), 2899-2938.

Chen, X., & Gunzburger, M. (2011). Continuous and discontinuous finite element methods for a peridynamics model of mechanics. *Computer Methods in Applied Mechanics and Engineering, 200*(9), 1237-1250.

Chen, Z., Bunger, A., Zhang, X., & Jeffrey, R. G. (2009). Cohesive zone finite element-based modeling of hydraulic fractures. *Acta Mechanica Solida Sinica, 22*(5), 443-452.

Cook, B., Lee, M., DiGiovanni, A., Bronowski, D., Perkins, E., & Williams, J. (2004). Discrete element modeling applied to laboratory simulation of near-wellbore mechanics. *International Journal of Geomechanics, 4*(1), 19-27.

Cundall, P. A., & Strack, O. D. (1979). A discrete numerical model for granular assemblies. *Geotechnique, 29*(1), 47-65.

Demmie, P. N., & Silling, S. A. (2007). An approach to modeling extreme loading of structures using peridynamics. *Journal of Mechanics of Materials and Structures, 2*(10), 1921-1945.

Donzé, F. V., Richefeu, V., & Magnier, S.-A. (2009). Advances in discrete element method applied to soil, rock and concrete mechanics. State of the art of geotechnical engineering. *Electronic Journal of Geotechnical Engineering, 44*, 31.

Du, Q., Gunzburger, M., Lehoucq, R. B., & Zhou, K. (2012). Analysis and approximation of nonlocal diffusion problems with volume constraints. *SIAM Review, 54*(4), 667-696.

Du, Q., Kamm, J. R., Lehoucq, R. B., & Parks, M. L. (2012). A new approach for a nonlocal, nonlinear conservation law. *SIAM Journal on Applied Mathematics, 72*(1), 464-487.

Dugdale, D. (1960). Yielding of steel sheets containing slits. *Journal of the Mechanics and Physics of Solids, 8*(2), 100-104.

Dullien, F. A. (1991). *Porous media: fluid transport and pore structure*: Academic Press, Waterloo.

Fisher, M. K., Wright, C. A., Davidson, B. M., Steinsberger, N. P., Buckler, W. S., Goodwin, A., & Fielder, E. O. (2005). Integrating fracture mapping technologies to improve stimulations in the Barnett Shale. *SPE Production & Facilities, 20*(02), 85-93.

Fu, P., Johnson, S. M., & Carrigan, C. R. (2013). An explicitly coupled hydro-geomechanical model for simulating hydraulic fracturing in arbitrary discrete fracture networks. *International Journal for Numerical and Analytical Methods in Geomechanics, 37*(14), 2278-2300.

Garagash, D. I. (2006). Propagation of a plane-strain hydraulic fracture with a fluid lag: early-time solution. *International Journal of Solids and Structures, 43*(18), 5811-5835.

Gerstle, W., Sakhavand, N., & Chapman, S. (2010). Peridynamic and continuum models of reinforced concrete lap splice compared. *Fracture Mechanics of Concrete and Concrete Structures - Recent Advances in Fracture Mechanics of Concrete,* ISBN 978-89-5708-180-8.

Gerstle, W., Sau, N., & Aguilera, E. (2007a). *Micropolar peridynamic constitutive model for concrete.* Paper presented at the 19th International Conference of Structural Mechanics in Reactor Technology. Toronto Canada.

Gerstle, W., Sau, N., & Aguilera, E. (2007b). *Micropolar peridynamic constitutive model for concrete.* Paper presented at the 19th International Conference on Structural Mechanics in Reactor Technology (SMiRT 19).

Gerstle, W., Sau, N., & Sakhavand, N. (2009). On peridynamic computational simulation of concrete structures. *ACI Special Publication, 265*.

Gerstle, W., Sau, N., & Silling, S. (2007). Peridynamic modeling of concrete structures. *Nuclear Engineering and Design, 237*(12), 1250-1258.

Ghassemi, A., & Diek, A. (2002). Porothermoelasticity for swelling shales. *Journal of Petroleum Science and Engineering, 34*(1), 123-135.

Ghassemi, A., Tarasovs, S., & Cheng, A.-D. (2007). A 3-D study of the effects of thermomechanical loads on fracture slip in enhanced geothermal reservoirs. *International Journal of Rock Mechanics and Mining Sciences, 44*(8), 1132-1148.

Gu, H., Weng, X., Lund, J. B., Mack, M. G., Ganguly, U., & Suarez-Rivera, R. (2011). *Hydraulic fracture crossing natural fracture at non-orthogonal angles, a criterion, its validation and applications.* Paper presented at the SPE Hydraulic Fracturing Technology Conference.

Ha, Y. D., & Bobaru, F. (2011). Characteristics of dynamic brittle fracture captured with peridynamics. *Engineering Fracture Mechanics, 78*(6), 1156-1168.

Hentz, S., Donzé, F. V., & Daudeville, L. (2004). Discrete element modelling of concrete submitted to dynamic loading at high strain rates. *Computers & Structures, 82*(29), 2509-2524.

Holyland, P., & Ojala, V. (1997). Computer-aided structural targeting in mineral exploration: two-and three-dimensional stress mapping. *Australian Journal of Earth Sciences, 44*(4), 421-432.

Honarvar Gheitanbaf, H. (2013). *Parallel simulation of particle dynamics with application to micropolar peridynamic lattice modeling of reinforced concrete structures (Thesis of master of science, Civil Engineering)*, Retrieved from The University of New Mexico Albuquerque, New Mexico, Database.

Hossain, M., Rahman, M., & Rahman, S. (2002). A shear dilation stimulation model for production enhancement from naturally fractured reservoirs. *SPE Journal, 7*(02), 183-195.

Hu, W., Ha, Y. D., & Bobaru, F. (2012). Peridynamic model for dynamic fracture in unidirectional fiber-reinforced composites. *Computer Methods in Applied Mechanics and Engineering, 217*, 247-261.

Hu, Y., Yu, Y., & Wang, H. (2014). Peridynamic analytical method for progressive damage in notched composite laminates. *Composite Structures, 108*, 801-810.

Hunsweck, M. J., Shen, Y., & Lew, A. J. (2013). A finite element approach to the simulation of hydraulic fractures with lag. *International Journal for Numerical and Analytical Methods in Geomechanics, 37*(9), 993-1015.

Hunt, S. P., Meyers, A., & Louchnikov, V. (2003). Modelling the Kaiser effect and deformation rate analysis in sandstone using the discrete element method. *Computers and Geotechnics, 30*(7), 611-621.

Jiang, Z., Oliver, N. H., Barr, T. D., Power, W. L., & Ord, A. (1997). Numerical modeling of fault-controlled fluid flow in the genesis of tin deposits of the Malage ore field, Gejiu mining district, China. *Economic Geology, 92*(2), 228-247.

Jing, L., & Stephansson, O. (2007). *Fundamentals of discrete element methods for rock engineering: theory and applications* (Vol. 85): Elsevier, Amesterdam.

Katiyar, A., Foster, J. T., Ouchi, H., & Sharma, M. M. (2014). A peridynamic formulation of pressure driven convective fluid transport in porous media. *Journal of Computational Physics, 261*, 209-229.

Kilic, B. (2008). *Peridynamic theory for progressive failure prediction in homogeneous and heterogeneous materials*: ProQuest.

Kilic, B., & Madenci, E. (2009). Structural stability and failure analysis using peridynamic theory. *International Journal of Non-Linear Mechanics, 44*(8), 845-854.

Kilic, B., & Madenci, E. (2010). Peridynamic theory for thermomechanical analysis. *Advanced Packaging, IEEE Transactions on, 33*(1), 97-105.

King, G. E., Haile, L., Shuss, J. A., & Dobkins, T. (2008). *Increasing fracture path complexity and controlling downward fracture growth in the Barnett shale.* Paper presented at the SPE Shale Gas Production Conference.

Le Calvez, J. H., Craven, M. E., Klem, R. C., Baihly, J. D., Bennett, L. A., & Brook, K. (2007). *Real-time microseismic monitoring of hydraulic fracture treatment: a tool to improve completion and reservoir management.* Paper presented at the SPE Hydraulic Fracturing Technology Conference.

Le Guen, C., Deveughele, M., Billiotte, J., & Brulhet, J. (1993). Gas permeability changes of rocksalt subjected to thermo-mechanical stresses. *Quarterly Journal of Engineering Geology and Hydrogeology, 26*(4), 327-334.

Lecampion, B., & Detournay, E. (2007). An implicit algorithm for the propagation of a hydraulic fracture with a fluid lag. *Computer Methods in Applied Mechanics and Engineering, 196*(49), 4863-4880.

Madenci, E., & Oterkus, E. (2014). *Peridynamic theory and its applications*: Springer, New York.

Manual, P. D. U. s. (1995). Itasca Consulting Group. *Inc., Minneapolis, Minnesota, USA*.

Matthäi, S. K., & Roberts, S. G. (1997). Transient versus continuous fluid flow in seismically active faults: an investigation by electric analogue and numerical modelling. In *Fluid Flow and Transport in Rocks* (pp. 263-295): Springer, London.

McLennan, J. D., Tran, D. T., Zhao, N., Thakur, S. V., Deo, M. D., Gil, I. R., & Damjanac, B. (2010). *Modeling fluid invasion and hydraulic fracture propagation in naturally fractured formations: a three-dimensional approach.* Paper presented at the SPE International Symposium and Exhibiton on Formation Damage Control.

Morris, K. (1980). Comparison of major sequences of organic-rich mud deposition in the British Jurassic. *Journal of the Geological Society, 137*(2), 157-170.

Nadimi, S., Shahriar, K., Sharifzadeh, M., & Moarefvand, P. (2011). Triaxial creep tests and back analysis of time-dependent behavior of Siah Bisheh cavern by 3-Dimensional Distinct Element Method. *Tunnelling and Underground Space Technology, 26*(1), 155-162.

Nadimi, S., Gomar, M., & Shahriar, K. (2013). Finite element modeling of borehole breakouts: initiation, propagation and stabilization. *23rd International Mining Congress & Exhibition,* Turkey, Antalya, 1291-1297.

Nadimi, S., & Miskovic, I. (2015). A peridynamic simulation of hydraulic fracture phenomena in shale reservoirs *GEOPROC Conference, 1*.

Nadimi, S., & Shahriar, K. (2014). Experimental creep tests and prediction of long-term creep behavior of grouting material. *Arabian Journal of Geosciences, 7*(8), 3251-3257.

Nadimi, S., Shahriar, K., Sharifzade, M., & Moarefvan, P. (2010). *Numerical analysis of time-dependent behavior of siah bisheh cavern.* Paper presented at the ISRM International Symposium-6th Asian Rock Mechanics Symposium.

Narasimhan, T. (1982). Multidimensional numerical simulation of fluid flow in fractured porous media. *Water Resources Research, 18*(4), 1235-1247.

Nguetseng, G. (1989). A general convergence result for a functional related to the theory of homogenization. *SIAM Journal on Mathematical Analysis, 20*(3), 608-623.

Oliver, N. H., & Bons, P. D. (2001). Mechanisms of fluid flow and fluid–rock interaction in fossil metamorphic hydrothermal systems inferred from vein–wallrock patterns, geometry and microstructure. *Geofluids, 1*(2), 137-162.

Oliver, N. H., Ord, A., Valenta, R., & Upton, P. (2001). Deformation, fluid flow, and ore genesis in heterogeneous rocks, with examples and numerical models from the Mount Isa district, Australia. *Reviews in Economic Geology, 14*, 51-71.

Olson, J. (2008). *Multi-fracture propagation modeling: Applications to hydraulic fracturing in shales and tight gas sands.* Paper presented at the The 42nd US rock mechanics symposium (USRMS).

Ortiz, M., & Pandolfi, A. (1999). Finite-deformation irreversible cohesive elements for three-dimensional crack-propagation analysis. *International Journal for Numerical Methods in Engineering, 44*(9), 1267-1282.

Oterkus, S., Madenci, E., & Agwai, A. (2014). Peridynamic thermal diffusion. *Journal of Computational Physics, 265*, 71-96.

Park, N., Holder, J., & Olson, J. (2004). *Discrete element modeling of fracture toughness tests in weakly cemented sandstone.* Paper presented at the Gulf Rocks 2004 the 6th North America Rock Mechanics Symposium (NARMS).

Passey, Q. R., Bohacs, K., Esch, W. L., Klimentidis, R., & Sinha, S. (2010a). *From oil-prone source rock to gas-producing shale reservoir-geologic and petrophysical characterization of unconventional shale gas reservoirs.* Paper presented at the International oil and gas conference and exhibition in China.

Passey, Q. R., Bohacs, K., Esch, W. L., Klimentidis, R., & Sinha, S. (2010b). *From oil-prone source rock to gas-producing shale reservoir–geologic and petrophysical characterization of unconventional shale-gas reservoirs.* Paper pressented at the CPS/SPE international conference in Beijing, China.

Phillips, O. M. (1991). *Flow and reactions in permeable rocks*: Cambridge University Press, Great Britain.

Plimpton, S., Thompson, A., & Crozier, P. LAMMPS Molecular Dynamics Simulator. 2014.

Potyondy, D., & Cundall, P. (2004). A bonded-particle model for rock. *International Journal of Rock Mechanics and Mining Sciences, 41*(8), 1329-1364.

Potyondy, D., Cundall, P., & Lee, C. (1996). *Modelling rock using bonded assemblies of circular particles.* Paper presented at the 2nd North American Rock Mechanics symposium.

Rabczuk, T., & Belytschko, T. (2004). Cracking particles: a simplified meshfree method for arbitrary evolving cracks. *International Journal for Numerical Methods in Engineering, 61*(13), 2316-2343.

Rahman, M., & Rahman, M. (2010). A review of hydraulic fracture models and development of an improved pseudo-3D model for stimulating tight oil/gas sand. *Energy Sources, Part A: Recovery, Utilization, and Environmental Effects, 32*(15), 1416-1436.

Revil, A., & Leroy, P. (2004). Constitutive equations for ionic transport in porous shales. *Journal of Geophysical Research: Solid Earth (1978–2012), 109*(B3).

Rijken, P., & Cooke, M. L. (2001). Role of shale thickness on vertical connectivity of fractures: application of crack-bridging theory to the Austin Chalk, Texas. *Tectonophysics, 337*(1), 117-133.

Rougier, E., Munjiza, A., & John, N. (2004). Numerical comparison of some explicit time integration schemes used in DEM, FEM/DEM and molecular dynamics. *International Journal for Numerical Methods in Engineering, 61*(6), 856-879.

Rutqvist, J., Wu, Y.-S., Tsang, C.-F., & Bodvarsson, G. (2002). A modeling approach for analysis of coupled multiphase fluid flow, heat transfer, and deformation in fractured porous rock. *International Journal of Rock Mechanics and Mining Sciences, 39*(4), 429-442.

Sakhavand, N. (2011). *Parallel simulation of reinforced concrete sructures using peridynamics (Thesis of master of science, Civil Engineering)*, Retrieved from The University of New Mexico Albuquerque, New Mexico, Database.

Shapiro, S. A., & Müller, T. M. (1999). Seismic signatures of permeability in heterogeneous porous media. *Geophysics, 64*(1), 99-103.

Shapiro, S. A., Rothert, E., Rath, V., & Rindschwentner, J. (2002). Characterization of fluid transport properties of reservoirs using induced microseismicity. *Geophysics, 67*(1), 212-220.

Sheng, Y., Lawrence, C., Briscoe, B., & Thornton, C. (2004). Numerical studies of uniaxial powder compaction process by 3D DEM. *Engineering Computations, 21*(2/3/4), 304-317.

Shin, D. H. (2013). Simultaneous propagation of multiple fractures in a horizontal well *(Thesis of master of science in Engineering, Petroleum and Geosystems Engineering,)*, Retrieved from The University of Texas at Austin, UT Electronic Theses and Dissertations.

Silling, S. (1998). Reformation of elasticity theory for discontinuous and long-range forces. *SAND98-2176, Sandia National Laboratories, Albuquerque, NM.*

Silling, S. (2003). Dynamic fracture modeling with a meshfree peridynamic code. *Computational Fluid and Solid Mechanics, 2003*, 641-644.

Silling, S., & Lehoucq, R. (2010). Peridynamic theory of solid mechanics. *Advances in Applied Mechanics, 44*, 73-168.

Silling, S. A. (2000). Reformulation of elasticity theory for discontinuities and long-range forces. *Journal of the Mechanics and Physics of Solids, 48*(1), 175-209.

Silling, S. A., & Askari, E. (2005). A meshfree method based on the peridynamic model of solid mechanics. *Computers & Structures, 83*(17), 1526-1535.

Silling, S. A., & Bobaru, F. (2005). Peridynamic modeling of membranes and fibers. *International Journal of Non-Linear Mechanics, 40*(2), 395-409.

Silling, S. A., Epton, M., Weckner, O., Xu, J., & Askari, E. (2007). Peridynamic states and constitutive modeling. *Journal of Elasticity, 88*(2), 151-184.

Song, J. H., Areias, P., & Belytschko, T. (2006). A method for dynamic crack and shear band propagation with phantom nodes. *International Journal for Numerical Methods in Engineering, 67*(6), 868-893.

Suarez-Rivera, R., Green, S. J., McLennan, J., & Bai, M. (2006). *Effect of layered heterogeneity on fracture initiation in tight gas shales.* Paper presented at the SPE Annual Technical Conference and Exhibition.

Suarez-Rivera, R., Handwerger, D., Kieschnick, J., Martin, W., & Green, S. (2005). *Accounting for heterogeneity provides a new perspective for completions in tight gas shales.* Paper presented at the Alaska Rocks 2005 The 40th US Symposium on Rock Mechanics (USRMS).

Taylor, M., & Steigmann, D. J. (2013). A two-dimensional peridynamic model for thin plates. *Mathematics and Mechanics of Solids*, 1081286513512925.

Terzaghi, K. (1943). *Theoretical soil mechanics*. Wiley, New York.

Tuniki, B. K. (2012). *Peridynamic constitutive model for concrete (Thesis of master of science, Civil Engineering)*, Retrieved from The University of New Mexico Albuquerque, New Mexico, Database.

Turner, D. Z. (2013). A non-local model for fluid-structure interaction with applications in hydraulic fracturing. *International Journal for Computational Methods in Engineering Science and Mechanics, 14*(5), 391-400.

Valk, P., & Economides, M. J. (1995). *Hydraulic fracture mechanics*: Wiley, New York.

Wang, S., Sun, L., Au, A., Yang, T., & Tang, C. (2009). 2D-numerical analysis of hydraulic fracturing in heterogeneous geo-materials. *Construction and Building Materials, 23*(6), 2196-2206.

Warpinski, N., & Teufel, L. (1987). Influence of geologic discontinuities on hydraulic fracture propagation (includes associated papers 17011 and 17074). *Journal of Petroleum Technology, 39*(02), 209-220.

Warren, T. L., Silling, S. A., Askari, A., Weckner, O., Epton, M. A., & Xu, J. (2009). A non-ordinary state-based peridynamic method to model solid material deformation and fracture. *International Journal of Solids and Structures, 46*(5), 1186-1195.

Weijers, L. (1995). *The near-wellbore geometry of hydraulic fractures initiated from horizontal and deviated wells.* TU Delft, Delft University of Technology.

Weng, X., Kresse, O., Cohen, C.-E., Wu, R., & Gu, H. (2011). Modeling of hydraulic-fracture-network propagation in a naturally fractured formation. *SPE Production & Operations, 26*(04), 368-380.

Whitsitt, N., & Dysart, G. (1970). The effect of temperature on stimulation design. *Journal of Petroleum Technology, 22*(04), 493-502.

Xiang, J. (2011). *A PKN hydraulic fracture model study and formation permeability determination.* Texas A&M University.

Xu, J., Askari, A., Weckner, O., & Silling, S. (2008). Peridynamic analysis of impact damage in composite laminates. *Journal of Aerospace Engineering, 21*(3), 187-194.

Yang, D., Sheng, Y., Ye, J., & Tan, Y. (2011). Dynamic simulation of crack initiation and propagation in cross-ply laminates by DEM. *Composites Science and Technology, 71*(11), 1410-1418.

Yew, C. H. (1997). *Mechanics of hydraulic fracturing*: Gulf Professional Publishing, Amsterdam.

Yu, K., Xin, X., & Lease, K. (2011). A new adaptive integration method for the peridynamic theory. *Modelling and Simulation in Materials Science and Engineering, 19*(4), 045003.

Yu, Y., & Wang, H. (2014). Peridynamic analytical method for progressive damage in notched composite laminates. *Composite Structures, 108*, 801-810.

Zhang, X., Thiercelin, M. J., & Jeffrey, R. G. (2007). *Effects of frictional geological discontinuities on hydraulic fracture propagation.* Paper presented at the SPE Hydraulic Fracturing Technology Conference.

Zhou, F., & Molinari, J.-F. (2004). Dynamic crack propagation with cohesive elements: a methodology to address mesh dependency. *International Journal for Numerical Methods in Engineering, 59*(1), 1-24.

Zhou, J., Chen, M., Jin, Y., & Zhang, G.-q. (2008). Analysis of fracture propagation behavior and fracture geometry using a tri-axial fracturing system in naturally fractured reservoirs. *International Journal of Rock Mechanics and Mining Sciences, 45*(7), 1143-1152.

Zhou, X., & Ghassemi, A. (2009). Finite element analysis of coupled chemo-poro-thermo-mechanical effects around a wellbore in swelling shale. *International Journal of Rock Mechanics and Mining Sciences, 46*(4), 769-778.

Zoback, M., Rummel, F., Jung, R., & Raleigh, C. (1977). *Laboratory hydraulic fracturing experiments in intact and pre-fractured rock.* Paper presented at the International Journal of Rock Mechanics and Mining Sciences & Geomechanics Abstracts.